CO_2-dependent opening of Connexin 43 hemichannels

Valentin-Mihai Dospinescu*, Alexander Mascarenhas*, Jack Butler, Sarbjit Nijjar, Kyara de Oliveira Taborda, Sean Connors, Lumei Huang and Nicholas Dale+.

School of Life Sciences, University of Warwick, Coventry, CV4 7AL, UK

* Co-first authors

+ Corresponding author: N.E.Dale@warwick.ac.uk

Key words: connexin, CO_2, hemichannel, carbamylation, carboxylation

Abstract

Sequence and structure comparisons between alpha and beta connexins, Cx43 and Cx26, revealed that Cx43 has a motif, the carbamylation motif, that confers CO_2-sensitivity on a subset of beta connexins. By using a fluorescent dye loading assay, whole cell patch clamp recordings and real time measurement of ATP release via $GRAB_{ATP}$ we have demonstrated that Cx43 hemichannels open in a highly CO_2 sensitive manner over the range 20 to 70 mmHg. Mutational analysis confirms that the equivalent residues to those in Cx26 that have been shown to be involved in mediating the effects of CO_2 on gating of hemichannels and gap junction channels, also mediate Cx43 hemichannel gating. Our data predicts that Cx43 will be partially open and able to release ATP at resting physiological levels of PCO_2. We have tested this prediction in acute hippocampal slices, by showing that CO_2-dependent enhancement of synaptic transmission can be blocked by the Cx43-selective mimetic peptide Gap26. Our data resolves an inconsistency in the literature between *in vivo* studies suggesting that Cx43 hemichannels are at least partially open at rest, and *in vitro* studies, performed in the absence of HCO_3^-/CO_2 buffering that show Cx43 hemichannels are shut. Our evidence suggests that the ancestral gene that duplicated to give the alpha and beta connexin clades must have possessed the carbamylation motif. CO_2 sensitivity is thus a fundamental ancient characteristic of several connexins that has been lost in more recently derived members of this gene family.

Introduction

There are 21 connexin genes encoded in the human genome. Connexins are transmembrane proteins that can form hemichannels and gap junction channels. The existence of 21 isoforms suggests functional specialisation across the gene family (Sohl & Willecke, 2004). On the basis of molecular phylogeny, the connexins have been divided into 4 broad clades -the alpha, beta, and gamma and delta groupings (Mikalsen *et al.*, 2021).

Certain members of the β-clade, Cx26, Cx30 and Cx32, are directly sensitive to CO_2 (Huckstepp *et al.*, 2010; Dospinescu *et al.*, 2019). The mechanism of CO_2 sensitivity has best been studied in Cx26. While Cx26 hemichannels are opened in response to CO_2 (Huckstepp *et al.*, 2010), CO_2 closes Cx26 gap junction channels (Nijjar *et al.*, 2021). The CO_2-dependent gating of Cx26 hemichannels and gap junction channels involves carbamylation of a specific lysine, K125, which is part of a critical carbamylation motif, $_{125}$KVRIEGS$_{131}$ (Meigh *et al.*, 2013). This motif is essential for the CO_2-sensitivity of Cx26, as it allows the formation of a salt bridge between the carbamylated K125 and R104 of the neighbouring subunit (Meigh *et al.*, 2013). The formation of this "carbamate" bridge induces conformational changes, ultimately leading to the opening of the hemichannel or closing of the gap junction channel (Meigh *et al.*, 2013; Nijjar *et al.*, 2021; Brotherton *et al.*, 2022; Brotherton *et al.*, 2024). Mutation of K125 to arginine, an amino acid that cannot be carbamylated, or R104 to alanine so that it cannot form a carbamate bridge, removes the ability of CO_2 to open Cx26 hemichannels (Meigh *et al.*, 2013) or close Cx26 gap junction channels (Nijjar *et al.*, 2021). Furthermore, the introduction of the carbamylation motif into a CO_2-insensitive connexin, Cx31, results in CO_2-dependent hemichannel opening of Cx31 (Meigh *et al.*, 2013). Other members of the β-clade, Cx30 and Cx32, are also CO_2-sensitive, but have different sensitivity profiles (Huckstepp *et al.*, 2010; Dospinescu *et al.*, 2019). Evolutionary comparisons show that the carbamylation motif has been conserved over 400 million years (Dospinescu *et al.*, 2019) and appears to be a necessary and sufficient feature for the CO_2-sensitivity of connexins.

Sequence comparisons of the β-connexins and α-connexins, revealed the presence of a potential carbamylation motif within the α-connexin, Cx43. Cx43 has a motif ($_{144}$KVKMRGG$_{150}$) homologous to the motif in Cx26 ($_{125}$KVRIEGS$_{131}$) suggesting that it might also be sensitive to CO_2. In this study we show that Cx43 hemichannels are indeed directly sensitive to changes in the partial pressure of CO_2 (PCO_2) over the physiological concentration range. Unlike Cx26, the CO_2-dependent opening mechanism of Cx43 is more complex, involving additional residues beyond the homologs of K125 and R104. Our discovery that Cx43 hemichannels are directly CO_2 sensitive has major physiological implications and may explain why Cx43 hemichannels appear to be open under physiological conditions but closed *in vitro* where they are usually studied in the absence of CO_2/HCO_3^- buffers.

Results

Identification of a potential carbamylation motif in Cx43

Cx43, an alpha-connexin, possesses a carbamylation motif homologous to that of the beta-connexins (Fig 1A). AlphaFold3 (AF3) predicts a structure very close to the experimentally determined structures for Cx43 (Lee *et al.*, 2023a; Qi *et al.*, 2023) but has the advantage of including portions of the structure that have not been

experimentally resolved. This is a valid approach, as the *de novo* predictions by AF3 for the cytoplasmic loop of Cx26 have been supported by a recent experimentally-derived structure (Brotherton *et al.*, 2024). By performing alignments of the Cx43 and Cx26 AF3 structures (Fig 1B), we found that two residues in Cx43, K144 and K105, aligned with the residues in Cx26 that are essential for hemichannel opening to CO_2, K125 and R104 (Fig 1C). The predicted 3D orientation of the alpha-helices involved are positioned in a similar manner to allow potential interaction between K144 and K105 following carbamylation. Cx43 also presents another feature that is similar to Cx26: the high incidence of Lys residues. In Cx26, 5 lysine residues in the cytoplasmic loop can be carbamylated, suggesting an environment favourable for this to happen. The presence of multiple Lys residues in the cytoplasmic loop of Cx43 implies that the local environment may be conserved to facilitate the required pKa for CO_2 binding and carbamate bridge formation.

Cx43 hemichannels are opened by CO_2

We used an established dye-loading protocol, previously used for CO_2 connexin studies (Huckstepp *et al.*, 2010; Meigh *et al.*, 2013; Meigh *et al.*, 2014; de Wolf *et al.*, 2016; de Wolf *et al.*, 2017; Cook *et al.*, 2019; Dospinescu *et al.*, 2019; van de Wiel *et al.*, 2020), to test whether Cx43 hemichannels are CO_2 sensitive. We observed significant dye-loading in Cx43-expressing cells when exposed to a high CO_2 stimulus (70 mmHg) when starting from a baseline of 20 mmHg (MW test, PCO_2 20 vs 70 mmHg: $p = 0.008$, n=5, Fig 2A). We used a zero Ca^{2+} aCSF to unblock hemichannels as a positive control to demonstrate that for WT Cx43, the zero Ca^{2+} stimulus and 70 mmHg PCO_2 gave a similar amount of dye loading (MW test: p-value = 0.726, n=5).

To further support these findings, we next used whole cell patch clamp recordings from HeLa cells expressing Cx43 (Fig 2B). From a baseline of 35 mmHg PCO_2, an increase in an outward conductance was observed when switching to 55 or 70 mmHg aCSF (Fig 2B). On switching to 20 mmHg aCSF, a small conductance decrease was observed (Fig 2B). Untransfected parental HeLa cells did not display an increase in outward current to changes in PCO_2. However, some parental HeLa cells exhibited a slow increase in an inward current on transfer from 35 to 70 mmHg (Fig 2B). This was quite distinct from the outward current observed in Cx43 expressing cells (Fig 2B). Overall, the patch clamp data predicted a dose response that could be fitted by the Hill equation with a Hill coefficient of 6 and an EC_{50} of 43 mmHg.

To assess whether the CO_2-dependent opening of Cx43 resulted in ATP release, we co-transfected HeLa cells with the genetically encoded ATP sensor - $GRAB_{ATP}$ (Wu *et al.*, 2022). CO_2 dependent increase in ATP release was indeed observed (n=22, Fig 2C). We observed an increase in $GRAB_{ATP}$ fluorescence on going from 20 to 35 mmHg PCO_2 and further to 55 mmHg PCO_2 (Fig 2C). While ATP release at 70 mmHg was slightly less than that at 55 mmHg, it remained markedly higher than at 35 mmHg PCO_2 (Fig 2C). Cells transfected with $GRAB_{ATP}$ only, showed no release in response to any concentration of CO_2 applied (n=14, Fig 2D). Overall, our results show through three independent assays that Cx43 hemichannels are opened by modest changes in PCO_2 around the physiological norm (Fig 2). Once opened by CO_2, Cx43 hemichannels display permeability to ATP (Fig 2C).

Gap Junction Channels (GJCs) of Cx26 are closed by CO_2 also acting via the carbamylation motif. We therefore tested whether Cx43 GJCs might also be CO_2

sensitive by using a dye transfer assay (Nijjar *et al.*, 2021). Cx43 GJCs allowed equally fast permeation of dye at all levels of PCO_2 and therefore, unlike the hemichannel, were insensitive to CO_2 (Fig 2, figure supplement 1).

Identifying the residues required for CO_2-sensitivity of Cx43

Having established the dose-response characteristics of Cx43 to CO_2, we next examined the potential underlying mechanisms for CO_2-dependent gating via targeted mutagenesis of possible key residues, starting with the equivalents of those known to be involved in the CO_2-sensitivity of Cx26 (Fig 1).

Mutation of K144 to glutamine (K144Q), an amino acid that cannot be carbamylated, partially reduced the CO_2-sensitivity of the channel: the 70 mmHg stimulus resulted in significantly less increase in dye loading than the zero Ca^{2+} positive control (Fig 3A, MW test: $p = 0.048$, n=5). However, mutation of Lys105 to a non-charged residue (K105Q) resulted in hemichannels that gave a similar increase in dye loading to the zero Ca^{2+} positive control (Fig 3B, MW test: $p = 0.111$, n=5). In Cx26, mutation of the residues involved in carbamylation (K125 and R104) results in complete loss of CO_2 sensitivity (Meigh *et al.*, 2013; Nijjar *et al.*, 2021). The lack of such a complete effect on the CO_2 sensitivity of Cx43 implies that the mechanism is more complex and may involve further residues.

We further inspected the AF3 structure prediction and identified two further lysine residues of interest (Fig 3E). K109 in Cx43 aligns with K108 of Cx26, a residue known to be carbamylated and required for Cx26 gap junction closure (Nijjar *et al.*, 2025). AF3 also suggests that K109 could potentially interact with K234 following any carbamylation (Fig 3E). We therefore mutated both residues to Gln to test their possible involvement in CO_2 sensitivity. The dye-loading assay showed that K109Q remained CO_2 sensitive (Fig 3C MW test vs zero Ca^{2+} control, $p = 0.274$, n=5). However, the mutation K234Q displayed impaired CO_2 sensitivity (Fig 3D, MW test vs zero Ca^{2+} control: $p = 0.016$, n=5).

As the dye loading assay suggested that single mutations were on the whole rather ineffective in abolishing CO_2 sensitivity, we assayed ATP release via $GRAB_{ATP}$ to gain further supporting evidence. We found that CO_2-evoked ATP release remained dose dependent and very similar to the WT Cx43 in the K105Q (n=23) and K144Q (n=12) mutants (Fig 4A, C, Figure 4, figure supplement 1). Cx43 hemichannels with the K109Q mutation appeared to have their sensitivity to CO_2 shifted to lower values of PCO_2 (n=20), appearing to give maximal ATP release at 35 mmHg (Fig 4B,E, Fig 4 figure supplement 1). K234Q Cx43 hemichannels had greatly reduced sensitivity to CO_2 (n=15, Fig 4D, F).

CO_2 sensitivity of Cx43 involves multiple Lys residues.

As single Lys mutations mostly had partial effects on the CO_2 sensitivity of Cx43 hemichannels, we next mutated pairs of Lys residues. Using the dye loading assay we found that all combinations of paired mutations abolished CO_2 sensitivity relative to the zero Ca^{2+} control (Fig 5): K109Q, K144Q (MW test $p = 0.008$, n=5); K105Q, K144Q (MW test $p = 0.004$, n=5); K105Q, K109Q (MW test $p = 0.004$, n=5); K105Q, K234Q (MW test $p = 0.004$, n=5); and K144Q, K234Q (MW test $p = 0.004$, n=5). Using the $GRAB_{ATP}$ assay we confirmed that all of these double mutations also abolished CO_2-

dependent ATP release (MW test for all mutations, CO_2 vs high K^+ positive control $p < 10^{-6}$, Fig 6).

The effect of introducing negatively charged residues into the carbamylation motif

We next sought to mimic carbamylation by mutating Lys to Glu. This introduces into the motif the negative charge that would occur upon carbamylation of Lys. In the dye loading assay the mutation K144E resulted in a complete loss of CO_2 sensitivity while dye loading to zero Ca^{2+} was retained (MW test, 70 mmHg vs zero Ca^{2+}: $p = 0.008$, n=5, Fig 7B). The mutation K105E seemed to disrupt both the CO_2-dependent and the zero Ca^{2+} evoked dye loading (Fig 7A). K234E displayed impaired CO_2-dependent dye loading compared to that evoked by zero Ca^{2+} (MW test, 70 mmHg vs zero Ca^{2+}: $p = 0.048$, n=5, Fig. 7C).

Using the $GRAB_{ATP}$ assay, we found that each of these single Lys to Glu mutations disrupted CO_2-dependent ATP release, but did not prevent depolarisation evoked ATP release (Fig 8). This disruptive effect on CO_2 dependence might arise because introduction of the negative charge changes the local environment and makes it harder to carbamylate the other Lys residues.

As a change in PCO_2 would likely carbamylate more than one Lys residue simultaneously, we made the double mutation K105E and K109E. With the dye loading assay we found that even at a PCO_2 of 20 mmHg, the cells loaded with dye suggesting that the mutated hemichannels were constitutively open (Fig 9A, D). Increasing PCO_2 to 70 mmHg gave no further dye loading. To test whether the channels were open even at a PCO_2 of 20 mmHg, we used the general hemichannel blocker La^{3+} (100 µM) to show that this reduced the dye loading at 20 mmHg (Fig 9B, D, MW test: $p = 0.016$, n=5). We used the $GRAB_{ATP}$ assay to demonstrate that at 20 mmHg, the K105E, K109E mutation caused continual release of ATP that could be blocked by La^{3+} (Fig 9C, D, MW test 20 mmHg vs 20 mmHg + La^{3+}, $p=7.7\times10^{-7}$, n=16). This continual release of ATP at 20 mmHg was not evident from cells expressing WT Cx43, as application of 100 µM La^{3+} had no effect on the $GRAB_{ATP}$ fluorescence (Fig 9C, D).

Physiological role for CO_2-dependent ATP release via Cx43 from astrocytes

Cx43 hemichannels are CO_2 sensitive and are likely to be partially open at typical levels of PCO_2 in mammalian tissue. They could thus be able to release ATP under physiological resting conditions (35 mmHg PCO_2, Fig. 2). Considering the ubiquitous distribution of Cx43 in astrocytes (de Ceglia *et al.*, 2023) and the likely resting PCO_2 in the brain (Hogg *et al.*, 1984), we postulated that, barring external modulatory influences, Cx43 hemichannels could continually release low levels of ATP in the hippocampus. Indeed, there exists compelling evidence for astrocytic Cx43 hemichannels being partially open under resting physiological conditions *in vitro* in the hippocampus (Chever *et al.*, 2014). In this study when Cx43 hemichannels were blocked by the mimetic peptide, Gap26, there was a decrease synaptic strength of about 30% that was occluded by targetted knock out of astrocytic Cx43 expression (Chever *et al.*, 2014).

As many investigators state that Cx43 hemichannels are shut under physiological conditions, we tested whether the results of Chever et al (2014) could be explained by the CO_2 sensitivity of Cx43. We predicted that if PCO_2 were lowered sufficiently to

largely close Cx43, when PCO_2 was returned to the physiological norm, Cx43 should re-open and result in an increase of synaptic strength, presumably downstream of Cx43-dependent ATP release (Chever *et al.*, 2014). Because ATP can be rapidly broken down to adenosine in the extracellular space (Frenguelli *et al.*, 2007; Wall & Dale, 2013), which could then act at A1 receptors to inhibit transmission and give confounding effects, we used 8-CPT (8-cyclopentyltheophylline) to selectively block A1 receptors.

We preincubated hippocampal slices in 20 mmHg PCO_2 aCSF for 30 mins prior to recording fEPSP in area CA1 evoked by stimulation of the Schaffer colaterals. At constant extracellular pH, in the presence of 8-CPT, elevation of PCO_2 from 20 to 35 mmHg resulted in a 26% increase in EPSP (n=6, Fig 10A). To test whether this effect was mediated via CO_2-dependent opening of Cx43, we used 100 μM Gap26 to see whether this blocked the increase in fEPSP induced by 35 mmHg PCO_2. Once again the fEPSP increased by about 30% on transfer to 35 mmHg aCSF (Fig. 10B), and application of Gap26 reduced the fEPSP to below its baseline value (Fig 10B, D, Friedmann 2 way ANOVA: p=0.006, n=6). This was an effect specific to the Gap26 peptide as 100 μM of the scrambled peptide did not have significant effects on the amplitude of the fEPSP (Fig. 10C, D, Friedmann 2 way ANOVA: p=0.55, n=5).

Pathological mutations of Cx43 cause loss of CO_2 sensitivity

A prominent condition associated with mutations of Cx43 is occulodental digital dysplasia (ODDD) (Laird, 2014). This syndrome involves a range of conditions such as soft tissue fusion of the digits, abnormal craniofacial bone development, small eyes and loss of tooth enamel. Later in age conditions such as glaucoma, skin disease and neuropathies may become evident. To determine wether the loss of Cx43 CO_2-sensitivity may be a contributing factor to human disease, we studied two mutations, the Cx43 ODDD mutation L90V (Shibayama *et al.*, 2005; Lai *et al.*, 2006) and A44V which causes the skin condition, erythrokeratodermia variabilis et progressiva (EKVP) (Cocozzelli & White, 2019; Srinivas *et al.*, 2019). We found that the L90V mutation removed CO_2 sensitivity from Cx43 by both the dye loading assay and the $GRAB_{ATP}$ assay (Fig 11). The mutation A44V blocked CO_2 dependent ATP release (Fig 11).

Discussion

Hemichannels of Cx43 are CO_2 sensitive

In contrast to Cx26 expression, which is restricted to specific, small regions of the brain (Nagy *et al.*, 2001; Rash *et al.*, 2001; Nagy *et al.*, 2011), Cx43 serves as the principal astrocytic connexin, exhibiting widespread presence throughout the brain (Schulz *et al.*, 2015; Yin *et al.*, 2018; de Ceglia *et al.*, 2023). This widespread distribution, combined with our results, suggests that Cx43 gives the capacity for CO_2 sensitivity across the entire brain.

Our data from three independent assays (dye loading, measurement of ATP release and whole cell recordings) show that hemichannels of Cx43 open to modest changes in PCO_2. However, Cx43 gap junction channels are insensitive to these same changes in PCO_2. At physiological levels of PCO_2 Cx43 hemichannels are partially open and able to release ATP. This observation potentially resolves a puzzling inconsistency in the literature. Many biophysical recordings of Cx43 hemichannels, performed in simplified HEPES buffered salines without appreciable dissolved CO_2 or HCO_3^-,

document Cx43 hemichannels as being shut. By contrast, under physiological conditions both *in vitro* and *in vivo*, which necessarily involve CO_2-HCO_3^- buffering, the evidence suggests that Cx43 hemichannels are constitutively open to some extent (Chever *et al.*, 2014; Guillebaud *et al.*, 2020; Turovsky *et al.*, 2020). Continual ATP release from astrocytes via Cx43 has been shown to give a tone of ATP that enhances the strength of synaptic transmission in the hippoampus by about 20% (Chever *et al.*, 2014). Our data is highly complementary to these observations as we find an enhancement of fEPSP amplitude of about 30% when increasing PCO_2 from 20 to 35 mmHg. It is important to note that our experiments were performed under isohydric conditions and differ from a prior study that examined hypocapnia with simultaneous alkalinisation. This manipulation enhanced fEPSP strength through a reduction in extracellular adenosine and consequently less inhibition via A1 receptors (Dulla *et al.*, 2005).

While our data suggests that Cx43 hemichannels are sensitive to PCO_2 over the range 20-70 mmHg, there is an indication that there may be some CO_2-dependent inhibition of hemichannel opening above 55 mmHg. Slightly less ATP release was consistently seen at a PCO_2 of 70 mmHg compared to 55 mmHg. Furthermore, we cannot be sure that Cx43 hemichannels are completely shut at a PCO_2 of 20 mmHg, as it is not possible to reduce the PCO_2 further without changing to HEPES buffered salines. That Gap26 reduced synaptic transmission below the baseline amplitude recorded in slices bathed in 20 mmHg aCSF suggests that even under this condition there may still be a low level of Cx43 hemichannel gating at least in neural tissue which will continually generate CO_2 via oxidative phosphorylation.

The residues involved in CO_2 sensitivity and possible mechanisms

By exploiting the new structural data for connexins (Myers *et al.*, 2018; Flores *et al.*, 2020; Lee *et al.*, 2020; Yue *et al.*, 2021; Brotherton *et al.*, 2022; Qi *et al.*, 2022; Lee *et al.*, 2023a; Lee *et al.*, 2023b; Qi *et al.*, 2023), the predictive power of AF3 and our understanding of carbamylation and CO_2-dependent gating of Cx26 hemichannels and GJCs (Nijjar *et al.*, 2021; Brotherton *et al.*, 2024), we identified a series of residues that could plausibly be involved in mediating the CO_2 sensitivity of Cx43: K144, the equivalent of K125 in Cx26; K105, the analogue of R104 in Cx26; K109, the equivalent of K108 in Cx26; and K234, an equivalent of R216 in Cx26. Both K125 and K108 in Cx26 are known to be carbamylated (Nijjar *et al.*, 2025). Carbamylation of K125 is essential for hemichannel opening to CO_2, whereas carbamylation of both K125 and K108 is required for GJC closure to CO_2 (Nijjar *et al.*, 2025). R216 in Cx26 has been tentatively identified as a possible interacting partner for K108 but this could be indirect (Nijjar *et al.*, 2025). Crucially the spatial arrangements of K144, K105, K109 and K234 in AF3 predictions indicate that these residues are sufficiently close to interact across the subunit boundary.

In Cx26, K125 is proposed to interact with R104 following carbamylation, and interestingly mutation of either K125 or R104 is sufficient to abolish CO_2 dependent hemichannel opening and GJC closure. Mutation of K108 is also sufficient by itself to abolish GJC closure to CO_2 (Nijjar *et al.*, 2025). By contrast single mutations to Gln of any of the 4 Lys residues identified in Cx43 as the equivalents to those involved in CO_2-dependent gating of Cx26 were unable to completely abolish CO_2 sensitivity. Similarly the mutations K125E and R104E in Cx26 create consitutively open hemichannels. However single Lys to Glu mutations in Cx43 did not have this effect.

Our data show that in Cx43 at least 2 of the 4 identified residues must be mutated to completely abolish CO_2 sensitivity or to give constitutively open hemichannels. For example mutation of any two Lys residues to Gln, completely abolishes CO_2 dependent ATP release and dye loading. Conversely the double mutation, K105E and K109E, is required for constitutively open hemichannels.

This suggests that in Cx43 there is some redundancy in the effect of CO_2. One possible interpretation is that two carbamate bridges are formed: one being between K144 and K105 (the direct equivalent of K125-R104 in Cx26); and the second being between K109 and K234. There is certainly some data that support this: the double mutations K109Q-K144Q, K105Q-K234Q and K144Q-K234Q being completely insensitive to CO_2. These double mutations would remove both of the proposed bridges. However our observation that the mutations K105Q-K144Q, K109Q-K234Q also completely remove CO_2 sensitivity is inconsistent with a simple two bridge hypothesis as these double mutations would only affect one of the bridges and should therefore leave the other intact to give some degree of CO_2 sensitivity. Instead, we favour a hypothesis in which any of these four residues could be carbamylated but that they all have potential to interact. Depending on which residues become carbamylated a bridge could form between K105 and K234 or between K109 and K144, and possibly even K144 and K234. There is some support for this idea from AF3 as K105 and K109 are only one turn distant in an alpha helix and both could therefore interact with either K144 or K234 following carbamylation. The residues in Cx43 that are involved in CO_2 sensitivity are equivalent to those identified in Cx26, where they participate in both hemichannel and gap junction channel gating to CO_2. However in Cx43 these residues are only involved in mediating the sensitivity of the hemichannel to CO_2. In this respect it is interesting that mutations of the different Lys residues alter the dose-sensitivity of Cx43 to CO_2 in different ways (Fig 4, figure supplement 1).

Physiological implications of the CO_2 sensitivity of Cx43

Cx43 is the most widely expressed connexin in the human body, being present in every organ system (Lucaciu *et al.*, 2023). In metabolically highly active organs such as liver, kidney and brain, ouir data suggest that the physiological PCO_2 will be sufficient to substantially open Cx43 hemichannels (Hogg *et al.*, 1984). In the context of the brain, Cx43 is the main astrocytic connexin and is expressed in all subtypes (de Ceglia *et al.*, 2023). This would imply that CO_2-sensitivity mediated via Cx43 will extend to potentially all brain regions. As astrocytes are non-excitable, they are unlikely to become sufficiently depolarised for Cx43 hemichannels to open via voltage dependent gating. We suggest therefore, in non-excitable cells such as astrocytes, that variations in PCO_2 may be the most important physiological regulator of Cx43 hemichannel gating. For astrocytes, CO_2-dependent opening of Cx43 hemichannels is likely to result in the release of a mix of small, neurochemically significant molecules such as ATP, glutamate, D-serine and lactate, depending on their intracellular concentration.

Cx43 is also highly expressed in the heart, if a proportion of the population were to be in hemichannel form as opposed to GJCs (De Smet *et al.*, 2021), the newly-discovered CO_2 sensitivity of hemichannels may have profound implications for heart function given that cardiomyocytes are highly active, and will thus generate high levels of CO_2 through oxidative phosphorylation. There is a long-established link between CO_2 and

cardiac function with effects such as increased coronary blood flow in response to CO_2 as well as changes in myocardial contractile function (Crystal, 2015). CO_2 can even cause arrythmias (Zhang *et al.*, 2019).

NF-kappa B and innate immunity exhibit sensitivity to CO_2 (Cummins *et al.*, 2010; Keogh *et al.*, 2017). Macrophages are CO_2-sensitive, although at least some of this is indirect and via pH changes mediated by carbonic anhydrase activity (Strowitzki *et al.*, 2022). However, a direct effect of CO_2 on components of the immune system cannot be excluded. In cell culture, when carbonic anhydrase activity is blocked in THP-1 monocytes, the effects of CO_2 are significantly diminished but not abolished, suggesting the existence of a pH-independent pathway (Strowitzki *et al.*, 2022). As Cx43 is expressed in monocytes it is a plausible candidate to mediate direct CO_2 sensitivity in these cells. Furthermore, Cx43 function in macrophages is deemed critical for various physiological and pathophysiological processes (Rodjakovic *et al.*, 2021). The role of CO_2 on such pathways remains to be explored.

It is interesting that pathological mutations of Cx43 abrogate CO_2 sensitivity. This follows a pattern seen for Cx26, where a range of mutations linked to syndromic and non-syndromic hearing loss (Meigh *et al.*, 2014; de Wolf *et al.*, 2016; Cook *et al.*, 2019), and for Cx32, where several mutations that cause X-linked Charcot Marie Tooth Disease (Butler & Dale, 2023) alter or completely block CO_2 sensitivity. Further studies are needed to see whether loss of CO_2 sensitivity from Cx43 does indeed contribute to pathology.

Evolution of CO_2 sensitivity in connexins

Our previous findings showed that a common carbamylation motif is prevalent across the beta-connexin clade and confers CO_2-sensitivity on the connexins that possess it (Dospinescu *et al.*, 2019). This motif for example is present in shark Cx32 (which is CO_2 sensitive). Humans and sharks last shared a common ancestor about 400-450 MYA. Our discovery that a very similar carbamylation motif is present in Cx43 and confers CO_2 sensitivity onto their hemichannels, suggests that this property must have been present in the ancestral connexin gene that predated the establishment of the alpha and beta connexin clades. Further work is needed to understand the evolution of the carbamylation motif and CO_2 sensitivity, but our observations indicate that it is an ancient feature within the molecular phylogeny of the connexins, rather than being a more recently derived feature restricted to the beta connexins.

Methods

Recording Solutions

Hypocapnic (20 mmHg PCO_2): 140 mM NaCl, 10 mM $NaHCO_3$, 1.25 mM NaH_2PO_4, 3mM KCl, 1 mM $MgSO_4$, 10 mM D-glucose and 2 mM $CaCl_2$. This was bubbled with a mix of 95%O_2/5% and balanced with sufficient pure O_2 from an oxygen concentrator to give a final pH of ~7.3.

Control (35 mmHg PCO_2): 124 mM NaCl, 26 mM $NaHCO_3$, 1.25 mM NaH_2PO_4, 3 mM KCl, 10 mM D-glucose, 1 mM $MgSO_4$, 2 mM $CaCl_2$. This was bubbled with 95%O_2/5% CO_2 and had a final pH of ~7.3.

Hypercapnic (55 mmHg PCO_2): 100 mM NaCl, 50 mM $NaHCO_3$, 1.25 mM NaH_2PO_4, 3 mM KCl, 10 mM D-glucose, 1 mM $MgSO_4$, 2 mM $CaCl_2$. This was bubbled with sufficient CO_2 (~9%, balance O_2) to give a final pH of ~7.3.

Hypercapnic (70 mmHg PCO_2): 73 mM NaCl, 80 mM $NaHCO_3$, 1.25 mM NaH_2PO_4, 3 mM KCl, 10 mM D-glucose, 1 mM $MgSO_4$, 2 mM $CaCl_2$. This was bubbled with sufficient CO_2 (approximately 12%, balance O_2) to give a final pH of ~7.3.

Zero Ca^{2+}: 140 mM NaCl, 10 mM $NaHCO_3$, 1.25 mM NaH_2PO_4, 3mM KCl, 1 mM $MgSO_4$. On the day of recording, 10 mM D-glucose and 2 mM $MgCl_2$ was added, and the solution bubbled with O_2 with a final pH of ~7.3.

Cell culture

HeLa DH cells were grown in Dulbecco's Modified Eagle Medium (DMEM), supplemented with 10% fetal bovine serum, 50 µg/mL penicillin/streptomycin. HeLa DH cells were used for patch clamp studies on Cx43 and for the dye loading of all Cx43 variants. For dye loading experiments, cells were seeded onto coverslips at a density of 7.5×10^4 cells per well and transiently transfected with the Cx43 constructs following the PEI Transfection Reagent protocol.

Dye-loading

Cell expressing the construct (48-72h) were given an initial 5-minute wash with control solution (artificial cerebrospinal fluid – aCSF, 20 mmHg PCO_2). Following this, the cells were exposed to either control solution, hypercapnic (70 mmHg PCO_2), or a zero Ca^{2+} control (20 mmHg PCO_2) solution, all of which contained 200 µM 5(6)-carboxyfluorescein (CBF) for 10 min. Next, cells were put into control solution with 200 µM CBF for 5 minutes to close any open channels and prevent dye loss in the next step. Then the coverslip was washed with control solution (without CBF) for another 30 min to remove extracellular dye. For each condition a different coverslip with HeLa cells was used. Cx43 was tagged with mCherry on the C-terminus using a short linker. Expression was verified using mCherry fluorescence. The experiments were replicated using independent transfections 5 times.

Following dye loading, HeLa cells were imaged by epifluorescence (Scientifica Slice Scope, Cairn Research OptoLED illumination, 60x water Olympus immersion objective, NA 1.0, Hamamatsu ImagEM EM-CCD camera, Metafluor software). CBFwas excited by a 470 nm LED, with emission captured between 504-543 nm. Cx43 constructs had a C-terminal mCherry tag, which was excited by a 535 nm LED and emission captured between 570-640 nm.

Following acquisition analysis was performed by a person blind to the experimental condition. ImageJ (Wayne Rasband, National Institutes of Health, USA) was used to measure the extent of dye loading by drawing a region of interest (ROI) around each cell, and subsequently, the mean pixel intensity of the ROI was determined. The mean pixel intensity of a representative background ROI for each image was subtracted from each cell measurement from the same image. At least 40 cells were measured for each condition per experiment, and five repetitions of independently transfected HeLa cells were completed. The mean pixel intensities were plotted as cumulative probability distributions, and these graphs show every data point measured. To assess the effect of the 70 mmHg and zero Ca^{2+} solutions on dye loading, the difference in

the median pixel intensities between the 70mmHg and 20 mmHg conditions, and the zero Ca^{2+} and 20 mmHg conditions was calculated for each transfection (Figs 3, 5, 7 and 11).

$GRAB_{ATP}$ recordings

Cells were transiently transfected with the pCAG-Cx43-mCherry construct and pDisplay-GRAB_ATP1.0-IRES-mCherry-CAAX (Addgene plasmid # 167582 ; RRID:Addgene_167582) (Wu *et al.*, 2022) 48 hours prior to imaging. Cells were perfused with control aCSF until a stable baseline was reached, before perfusion with either hypercapnic or high K^+ aCSF. Once a stable baseline was reached after solution change, cells were again perfused with control aCSF and when a stable baseline reached, recordings were calibrated by direct application of 3 μM of the corresponding analyte.

All cells were imaged by epifluorescence as above. The cpGFP in $GRAB_{ATP}$ was excited by a 470 nm LED, with emission captured between 504-543 nm. As the Cx43 constructs were mCherry tagged, we selected only cells that expressed both cpGFP and mCherry for recording. $GRAB_{ATP}$ fluorescence images were acquired every 4 seconds. For each condition, at least 3 independent transfections were performed with at least 2 coverslips per transfection.

Analysis of all experiments was carried out in ImageJ. Images were opened as a stack and stabilised. ROIs were drawn around cells co-expressing both sensor and connexin. Median pixel intensity was plotted as normalised fluorescence change ($\Delta F/F_0$) over time to give traces of fluorescence change. Amount of ATP release was quantified as concentration by normalising to the $\Delta F/F_0$ caused by application of 3 μM ATP.

Patch clamp recordings

Coverslips containing non-confluent HeLa cells were placed into a perfusion chamber at room temperature and superfused with control aCSF. An Axopatch 200B amplifier was used to make whole-cell recordings from single HeLa cells. The intracellular fluid in the patch pipettes contained: K-gluconate 60 mM, Cs-gluconate 50 mM, CsCl 10 mM, TEACl 10 mM, EGTA 10 mM, Na_2ATP 3mM, $MgCl_2$ 3 mM, $CaCl_2$ 1 mM, HEPES 10 mM, sterile filtered, pH adjusted to 7.2 with KOH. An agarose salt bridge was used to avoid solution changes altering the potential of the Ag/AgCl reference electrode. All whole-cell recordings were performed at a holding potential of -50 mV. Whole-cell conductance was measured by repeated steps to -40 mV. To allow for any drift in whole-cell conductance unrelated to the CO_2 stimulus, the maximal conductance during the CO_2 test stimulus was compared to the average of the conductance before the stimulus and after the stimulus had been fully washed off. Each whole cell recording was considered to be an independent statistical replicate.

Imaging assay of gap junction transfer

2-Deoxy-2-[(7-nitro-2,1,3-benzoxadiazol-4-yl)amino]-D-glucose, NBDG, was included at 200 μM in the patch recording fluid, which contained: K-gluconate 130 mM; KCl 10 mM; EGTA 5 mM; $CaCl_2$ 2 mM, HEPES 10 mM, pH was adjusted to 7.3 with KOH to give a resulting final osmolarity of 295 mOsm. Cells were imaged on a Cleverscope (MCI Neuroscience) with a Photometrics Prime camera under the control of Micromanager 1.4 software. LED illumination (Cairn Research) and an image splitter

(Optosplit, Cairn Research) allowed simultaneous imaging of the mCherry-tagged Cx43 subunits and the diffusion of the NBDG into and between cells. Coupled cells for intercellular dye transfer experiments were initially selected based on tagged Cx43 protein expression and the presence of a gap junctional plaque (Figure 4, figure supplement 1). Dye permeation between cells was measured at PCO_2 levels of 20, 55 and 70 mmHg. After establishing the whole cell mode of recording, images were collected every 10 seconds. The assay was performed as described by Nijjar et al (Nijjar *et al.*, 2021). The start of recording was taken to be the first image following the establishment of a stable whole cell recording. For each gap junction recording (considered as an independent statistical replicate), analysis of the cell images was performed in ImageJ using an ROI drawn on each cell to measure the median pixel intensity of the donor and acceptor cells. The time for the median fluorescence of the acceptor cell to reach 10% of the donor cell was then determined and used as the value for statistical comparisons.

Hippocampal slice preparation

Mice of either sex, 3-5 weeks old, were killed by cervical dislocation and decapitated in accordance with United Kingdom Animals (Scientific Procedures) Act (1986). The brain was dissected and kept on ice both the cerebellum and the rostral section of the brain were removed. 400 µm thick sagittal slices were cut with a vibratome (Microm HM 650V microsliver) in ice-cold cutting solution composed of (in mM: 85 NaCl, 2.5 KCl, 0.5 $CaCl_2$, 1.25 NaH_2PO_4, 24 $NaHCO_3$, 25 glucose, and 75 sucrose; pH was adjusted to 7.4, bubbled with 95% O_2 + 5% CO_2). Then slices were incubated in aCSF composed of (in mM: 127 NaCl, 1.9 KCl, 2 $MgCl_2$, 2 $CaCl_2$, 1.2 KH_2PO_4, 26 $NaHCO_3$, 10 D-glucose, pH 7.4, when bubbled with 95% O_2 and 5% CO_2) at 33 °C. For fEPSP recordings an individual slice was pre-incubated in 20 mmHg PCO_2 aCSF for 30 mins, following which the slice was transferred to a recording chamber submerged in aCSF at 32°C. For stimulation, pulses were delivered by a stimulator via concentric bipolar metal stimulating electrode placed on the surface of CA3. For extracellular recordings, an aCSF-filled microelectrode was placed in CA1.

Statistics

Data is plotted as either cumulative probabilities (showing every data point) or box and whisker plots where the box is interquartile rage, bar is median, and whisker extends to most extreme data point that is no more than 1.5 times the interquartile range. All individual data points are superimposed on the plots.

In the case of dye loading one transfection was considered one replicate. In the case of patch clamping and $GRAB_{ATP}$ experiments, one cell was considered one replicate. For dye-loading, to assess the effect a mutation would have on the protein, the difference in dye loading evoked by 70 mmHg PCO_2 or 0 Ca^{2+} conditions (from the 20 mmHg baseline) for each construct were compared, using the median value for each condition from each transfection. The Mann-Whitney U one-sided test was used for the comparison on the basis that *a priori* we expected mutations to either reduce CO_2 sensitivity or have no effect. To compare the fEPSP size across different conditions, the non-parametric Friedman two way ANOVA was used. Statistical analysis was performed using the python language and SciPy library.

Cloning

Plasmids were generated using the Gibson Assembly method (Gibson *et al.*, 2009). PCR fragments were amplified using Q5® High-Fidelity DNA Polymerase (New England Biolabs) (normal PCR or site-directed mutagenesis). The overlap region generated through PCR for Gibson Assembly was 20 base pairs, and the pCAG vector was used as the backbone. All PCR primers were purchased from Integrated DNA Technologies (IDT). All constructs were confirmed by DNA sequencing (Eurofins GATC sequencing or Plasmidasaurus).

Reagents used

Reagent type (species) or resource	Designation	Source or reference	Identifiers	Additional information
Chemical compound, drug	DMEM	Merck Life Sciences UK Ltd	CAT# D6046	
Chemical compound, drug	Fetal bovine serum	Labtech.com	CAT# FCS-SA	
Chemical compound, drug	GeneJuice Transfection Reagent	Merck Life Sciences UK Ltd	CAT# 70967-3	
Chemical compound, drug	Polyethylenimine			
Chemical compound, drug	5(6)-Carboxyfluorescein			
Chemical compound, drug	Opti-MEM™ I Reduced Serum Medium	Thermo Fisher Scientific	CAT# 31985070	
pDisplay-GRAB_ATP1.0	Plasmid	Addgene	plasmid#167582; RRID:Addgene_167582)	
Chemical compound, drug	GeneJuice	Merck Sigma-Aldrich	CAT# 70967	
Chemical compound, drug	5(6)-Carboxyfluorescein	Novabiochem	CAT# 8.51082	
Chemical compound, drug	2-Deoxy-2-[(7-nitro-2,1,3-benzoxadiazol-4-yl)amino]-D-glucose	AAT Bioquest	CAT# 36702	
Sequence-based reagent	Cx43-forward	IDT	PCRprimers	TACCGCGGGCCCGGGATCCACCGGTATGGGTGACTGGAGCGCC
Sequence-based reagent	Cx43-reverse	IDT	PCRprimers	GCGGTACCCCGATCTCCAGGTCATCAGGCC
Sequence-based reagent	mCherry-forward	IDT	PCRprimers	CCTGGAGATCGGGGTACCGCGGGCCCGG
Sequence-based reagent	mCherry-reverse	IDT	PCRprimers	CTTGATACTTACCTGCGGCCTCGAGTTA

				CTTGTACAGCTCGTCCATGCCGCCG
Sequence-based reagent	K105Q-forward	IDT	PCRprimers	GGAAGAGCAACTGAACAAGAAAGAGGAAG
Sequence-based reagent	K105Q-reverse	IDT	PCRprimers	TCTTGTTCAGTTGCTCTTCCTTTCGCATCACATAG
Sequence-based reagent	K109Q-forward	IDT	PCRprimers	GAACAAGCAAGAGGAAGAACTCAAGGTTGCCC
Sequence-based reagent	K109Q-reverse	IDT	PCRprimers	GTTCTTCCTCTTGCTTGTTCAGTTTCTCTTCCTTTCG
Sequence-based reagent	K144Q-forward	IDT	PCRprimers	GCATGGTCAGGTGAAAATGCGAGGGGGG
Sequence-based reagent	K144Q-reverse	IDT	PCRprimers	GCATTTTCACCTGACCATGCTCTTCAATACCGTAC
Sequence-based reagent	234Q-forward	IDT	PCRprimers	TTTCTTCCAGGGCGTTAAGGATCGGGTTAAGG
Sequence-based reagent	234Q-reverse	IDT	PCRprimers	CCTTAACGCCCTGGAAGAAAACATAGAAGAGTTCAATGATATTCAAG
Sequence-based reagent	105E-forward	IDT	PCRprimers	GGAAGAGGAACTGAACAAGAAAGAGGAAG
Sequence-based reagent	105E-reverse	IDT	PCRprimers	TCTTGTTCAGTTCCTCTTCCTTTCGCATCACATAG
Sequence-based reagent	144E-forward	IDT	PCRprimers	GCATGGTGAGGTGAAAATGCGAGGGGGG
Sequence-based reagent	144E-reverse	IDT	PCRprimers	GCATTTTCACCTCACCATGCTCTTCAATACCGTAC
Sequence-based reagent	234E-forward	IDT	PCRprimers	TTTCTTCGAGGGCGTTAAGGATCGGGTTAAGG
Sequence-based reagent	234E-reverse	IDT	PCRprimers	CCTTAACGCCCTCGAAGAAAACATAGAAGAGTTCAATGATATTCAAG
Sequence-based reagent	K105Q K109Q-forward	IDT	PCRprimers	GCAACTGAACAAGCAAGAGGAAGAACTCAAGGTTGCCC
Sequence-based reagent	K105Q K109Q-reverse	IDT	PCRprimers	GTTCTTCCTCTTGCTTGTTCAGTTGCTCTTCCTTTC
Sequence-based reagent	K105E K109E-forward	IDT	PCRprimers	GGAACTGAACAAGGAAGAGGAAGAACTCAAGGTTGCCC
Sequence-based reagent	K105E K109E-reverse	IDT	PCRprimers	GTTCTTCCTCTTCCTTGTTCAGTTCCTCTTCCTTTC

Software, algorithm	PyMol		https://pymol.org/	
Software, algorithm	AlphaFold3		https://alphafoldserver.com/	

Conflict of Interest

The authors declare that there are no conflicts of interest

Funding

We thank the BBSRC (BB/T013346/1, ND) for support. JB was supported by the Biotechnology and Biological Sciences Research Council (BBSRC) and University of Warwick funded Midlands Integrative Biosciences Training Partnership (MIBTP) grant number BB/T00746X/1. VMD was funded by the Medical Research Council through the University of Warwick Doctoral Training Partnership, grant number MR/N014294/1

Acknowledgements

We thank Prof Alexander Cameron for commenting on a draft of this paper.

References

Brotherton, D.H., Nijjar, S., Savva, C.G., Dale, N. & Cameron, A.D. (2024) Structures of wild-type and a constitutively closed mutant of connexin26 shed light on channel regulation by CO2. *eLife*, **13**, RP93686.

Brotherton, D.H., Savva, C.G., Ragan, T.J., Dale, N. & Cameron, A.D. (2022) Conformational changes and CO2-induced channel gating in connexin26. *Structure*, **30**, 697-706.

Butler, J. & Dale, N. (2023) X-linked Charcot Marie Tooth mutations alter CO(2) sensitivity of connexin32 hemichannels. *Front Cell Neurosci*, **17**, 1330983.

Chever, O., Lee, C.Y. & Rouach, N. (2014) Astroglial connexin43 hemichannels tune basal excitatory synaptic transmission. *J Neurosci*, **34**, 11228-11232.

Cocozzelli, A.G. & White, T.W. (2019) Connexin 43 Mutations Lead to Increased Hemichannel Functionality in Skin Disease. *Int J Mol Sci*, **20**.

Cook, J., de Wolf, E. & Dale, N. (2019) Cx26 keratitis ichthyosis deafness syndrome mutations trigger alternative splicing of Cx26 to prevent expression and cause toxicity in vitro. *Royal Society open science*, **6**, 191128.

Crystal, G.J. (2015) Carbon Dioxide and the Heart: Physiology and Clinical Implications. *Anesth Analg*, **121**, 610-623.

Cummins, E.P., Oliver, K.M., Lenihan, C.R., Fitzpatrick, S.F., Bruning, U., Scholz, C.C., Slattery, C., Leonard, M.O., McLoughlin, P. & Taylor, C.T. (2010) NF-kappaB links CO2 sensing to innate immunity and inflammation in mammalian cells. *J Immunol*, **185**, 4439-4445.

de Ceglia, R., Ledonne, A., Litvin, D.G., Lind, B.L., Carriero, G., Latagliata, E.C., Bindocci, E., Di Castro, M.A., Savtchouk, I., Vitali, I., Ranjak, A., Congiu, M., Canonica, T., Wisden, W., Harris, K., Mameli, M., Mercuri, N., Telley, L. & Volterra, A. (2023) Specialized astrocytes mediate glutamatergic gliotransmission in the CNS. *Nature*, **622**, 120-129.

De Smet, M.A., Lissoni, A., Nezlobinsky, T., Wang, N., Dries, E., Perez-Hernandez, M., Lin, X., Amoni, M., Vervliet, T., Witschas, K., Rothenberg, E., Bultynck, G., Schulz, R., Panfilov, A.V., Delmar, M., Sipido, K.R. & Leybaert, L. (2021) Cx43 hemichannel microdomain signaling at the intercalated disc enhances cardiac excitability. *The Journal of clinical investigation*, **131**.

de Wolf, E., Cook, J. & Dale, N. (2017) Evolutionary adaptation of the sensitivity of connexin26 hemichannels to CO2. *Proc R Soc B*, **284: 20162723**.

de Wolf, E., van de Wiel, J., Cook, J. & Dale, N. (2016) Altered CO2 sensitivity of connexin26 mutant hemichannels in vitro. *Physiol Rep*, **4**, e13038.

Dospinescu, V.-M., Nijjar, S., Spanos, F., Cook, J., de Wolf, E., Biscotti, M.A., Gerdol, M. & Dale, N. (2019) Structural determinants of CO2-sensitivity in the β connexin family suggested by evolutionary analysis. *Communications Biology*, **2**, 331.

Dulla, C.G., Dobelis, P., Pearson, T., Frenguelli, B.G., Staley, K.J. & Masino, S.A. (2005) Adenosine and ATP link PCO2 to cortical excitability via pH. *Neuron*, **48**, 1011-1023.

Flores, J.A., Haddad, B.G., Dolan, K.A., Myers, J.B., Yoshioka, C.C., Copperman, J., Zuckerman, D.M. & Reichow, S.L. (2020) Connexin-46/50 in a dynamic lipid environment resolved by CryoEM at 1.9 A. *Nat Commun*, **11**, 4331.

Frenguelli, B.G., Wigmore, G., Llaudet, E. & Dale, N. (2007) Temporal and mechanistic dissociation of ATP and adenosine release during ischaemia in the mammalian hippocampus. *J Neurochem*, **101**, 1400-1413.

Gibson, D.G., Young, L., Chuang, R.Y., Venter, J.C., Hutchison, C.A., 3rd & Smith, H.O. (2009) Enzymatic assembly of DNA molecules up to several hundred kilobases. *Nat Methods*, **6**, 343-345.

Guillebaud, F., Barbot, M., Barbouche, R., Brezun, J.M., Poirot, K., Vasile, F., Lebrun, B., Rouach, N., Dallaporta, M., Gaige, S. & Troadec, J.D. (2020) Blockade of Glial Connexin 43 Hemichannels Reduces Food Intake. *Cells*, **9**.

Hogg, R.J., Pucacco, L.R., Carter, N.W., Laptook, A.R. & Kokko, J.P. (1984) In situ PCO2 in the renal cortex, liver, muscle, and brain of the New Zealand white rabbit. *Am J Physiol*, **247**, F491-498.

Huckstepp, R.T., Eason, R., Sachdev, A. & Dale, N. (2010) CO2-dependent opening of connexin 26 and related beta connexins. *J Physiol*, **588**, 3921-3931.

Keogh, C.E., Scholz, C.C., Rodriguez, J., Selfridge, A.C., von Kriegsheim, A. & Cummins, E.P. (2017) Carbon dioxide-dependent regulation of NF-kappaB family members RelB and p100 gives molecular insight into CO(2)-dependent immune regulation. *J Biol Chem*, **292**, 11561-11571.

Lai, A., Le, D.N., Paznekas, W.A., Gifford, W.D., Jabs, E.W. & Charles, A.C. (2006) Oculodentodigital dysplasia connexin43 mutations result in non-functional connexin hemichannels and gap junctions in C6 glioma cells. *J Cell Sci*, **119**, 532-541.

Laird, D.W. (2014) Syndromic and non-syndromic disease-linked Cx43 mutations. *FEBS Lett*, **588**, 1339-1348.

Lee, H.-J., Jeong, H., Hyun, J., Ryu, B., Park, K., Lim, H.-H., Yoo, J. & Woo, J.-S. (2020) Cryo-EM structure of human Cx31.3/GJC3 connexin hemichannel. *Science Advances*, **6**, eaba4996.

Lee, H.J., Cha, H.J., Jeong, H., Lee, S.N., Lee, C.W., Kim, M., Yoo, J. & Woo, J.S. (2023a) Conformational changes in the human Cx43/GJA1 gap junction channel visualized using cryo-EM. *Nat Commun*, **14**, 931.

Lee, S.N., Cho, H.J., Jeong, H., Ryu, B., Lee, H.J., Kim, M., Yoo, J., Woo, J.S. & Lee, H.H. (2023b) Cryo-EM structures of human Cx36/GJD2 neuronal gap junction channel. *Nat Commun*, **14**, 1347.

Lucaciu, S.A., Leighton, S.E., Hauser, A., Yee, R. & Laird, D.W. (2023) Diversity in connexin biology. *J Biol Chem*, **299**, 105263.

Meigh, L., Greenhalgh, S.A., Rodgers, T.L., Cann, M.J., Roper, D.I. & Dale, N. (2013) CO2 directly modulates connexin 26 by formation of carbamate bridges between subunits. *eLife*, **2**, e01213.

Meigh, L., Hussain, N., Mulkey, D.K. & Dale, N. (2014) Connexin26 hemichannels with a mutation that causes KID syndrome in humans lack sensitivity to CO2. *eLife*, **3**, e04249.

Mikalsen, S.O., S, Í.K. & Tausen, M. (2021) Connexins during 500 Million Years-From Cyclostomes to Mammals. *Int J Mol Sci*, **22**.

Myers, J.B., Haddad, B.G., O'Neill, S.E., Chorev, D.S., Yoshioka, C.C., Robinson, C.V., Zuckerman, D.M. & Reichow, S.L. (2018) Structure of native lens connexin 46/50 intercellular channels by cryo-EM. *Nature*, **564**, 372-377.

Nagy, J.I., Li, X., Rempel, J., Stelmack, G., Patel, D., Staines, W.A., Yasumura, T. & Rash, J.E. (2001) Connexin26 in adult rodent central nervous system: demonstration at astrocytic gap junctions and colocalization with connexin30 and connexin43. *J Comp Neurol*, **441**, 302-323.

Nagy, J.I., Lynn, B.D., Tress, O., Willecke, K. & Rash, J.E. (2011) Connexin26 expression in brain parenchymal cells demonstrated by targeted connexin ablation in transgenic mice. *Eur J Neurosci*, **34**, 263-271.

Nijjar, S., Brotherton, D.H., Butler, J., Dospinescu, V.-M., Gannon, H., Linthwaite, V.L., Cann, M.J., Cameron, A. & Dale, N. (2025) Multiple carbamylation events are required for differential modulation of Cx26 hemichannels and gap junctions by CO_2. *The Journal of physiology*.

Nijjar, S., Maddison, D., Meigh, L., de Wolf, E., Rodgers, T., Cann, M.J. & Dale, N. (2021) Opposing modulation of Cx26 gap junctions and hemichannels by CO(2). *J Physiol*, **599**, 103-118.

Qi, C., Acosta Gutierrez, S., Lavriha, P., Othman, A., Lopez-Pigozzi, D., Bayraktar, E., Schuster, D., Picotti, P., Zamboni, N., Bortolozzi, M., Gervasio, F.L. & Korkhov, V.M. (2023) Structure of the connexin-43 gap junction channel in a putative closed state. *eLife*, **12**.

Qi, C., Acosta-Gutierrez, S., Lavriha, P., Othman, A., Lopez-Pigozzi, D., Bayraktar, E., Schuster, D., Picotti, P., Zamboni, N., Bortolozzi, M., Gervasio, F.L. & Korkhov, V.M. (2022) Structure of the connexin-43 gap junction channel reveals a closed sieve-like molecular gate. *bioRxiv*, 2022.2003.2026.485947.

Rash, J.E., Yasumura, T., Davidson, K.G., Furman, C.S., Dudek, F.E. & Nagy, J.I. (2001) Identification of cells expressing Cx43, Cx30, Cx26, Cx32 and Cx36 in gap junctions of rat brain and spinal cord. *Cell Commun Adhes*, **8**, 315-320.

Rodjakovic, D., Salm, L. & Beldi, G. (2021) Function of Connexin-43 in Macrophages. *Int J Mol Sci*, **22**.

Schulz, R., Gorge, P.M., Gorbe, A., Ferdinandy, P., Lampe, P.D. & Leybaert, L. (2015) Connexin 43 is an emerging therapeutic target in ischemia/reperfusion injury, cardioprotection and neuroprotection. *Pharmacol Ther*, **153**, 90-106.

Shibayama, J., Paznekas, W., Seki, A., Taffet, S., Jabs, E.W., Delmar, M. & Musa, H. (2005) Functional characterization of connexin43 mutations found in patients with oculodentodigital dysplasia. *Circ Res*, **96**, e83-91.

Sohl, G. & Willecke, K. (2004) Gap junctions and the connexin protein family. *Cardiovasc Res*, **62**, 228-232.

Srinivas, M., Jannace, T.F., Cocozzelli, A.G., Li, L., Slavi, N., Sellitto, C. & White, T.W. (2019) Connexin43 mutations linked to skin disease have augmented hemichannel activity. *Sci Rep*, **9**, 19.

Strowitzki, M.J., Nelson, R., Garcia, M.P., Tuffs, C., Bleul, M.B., Fitzsimons, S., Navas, J., Uzieliene, I., Ritter, A.S., Phelan, D., Kierans, S.J., Blanco, A., Bernotiene, E., Belton, O., Schneider, M., Cummins, E.P. & Taylor, C.T. (2022) Carbon Dioxide Sensing by Immune Cells Occurs through Carbonic Anhydrase 2-Dependent Changes in Intracellular pH. *J Immunol*, **208**, 2363-2375.

Turovsky, E.A., Braga, A., Yu, Y., Esteras, N., Korsak, A., Theparambil, S.M., Hadjihambi, A., Hosford, P.S., Teschemacher, A.G., Marina, N., Lythgoe, M.F., Haydon, P.G. & Gourine, A.V. (2020) Mechanosensory Signaling in Astrocytes. *J Neurosci*, **40**, 9364-9371.

van de Wiel, J., Meigh, L., Bhandare, A., Cook, J., Nijjar, S., Huckstepp, R. & Dale, N. (2020) Connexin26 mediates CO2-dependent regulation of breathing via glial cells of the medulla oblongata. *Communications Biology*, **3**, 521.

Wall, M.J. & Dale, N. (2013) Neuronal transporter and astrocytic ATP exocytosis underlie activity-dependent adenosine release in the hippocampus. *J Physiol*, **591**, 3853-3871.

Wu, Z., He, K., Chen, Y., Li, H., Pan, S., Li, B., Liu, T., Xi, F., Deng, F., Wang, H., Du, J., Jing, M. & Li, Y. (2022) A sensitive GRAB sensor for detecting extracellular ATP in vitro and in vivo. *Neuron*, **110**, 770-782 e775.

Yin, X., Feng, L., Ma, D., Yin, P., Wang, X., Hou, S., Hao, Y., Zhang, J., Xin, M. & Feng, J. (2018) Roles of astrocytic connexin-43, hemichannels, and gap junctions in oxygen-glucose deprivation/reperfusion injury induced neuroinflammation and the possible regulatory mechanisms of salvianolic acid B and carbenoxolone. *J Neuroinflammation*, **15**, 97.

Yue, B., Haddad, B.G., Khan, U., Chen, H., Atalla, M., Zhang, Z., Zuckerman, D.M., Reichow, S.L. & Bai, D. (2021) Connexin 46 and connexin 50 gap junction channel properties are shaped by structural and dynamic features of their N-terminal domains. *J Physiol*, **599**, 3313-3335.

Zhang, Q., Ma, J.H., Li, H., Wei, X.H., Zheng, J., Li, G., Wang, C.Y., Wu, Y., He, Q.H. & Wu, L. (2019) Increase in CO(2) levels by upregulating late sodium current is proarrhythmic in the heart. *Heart Rhythm*, **16**, 1098-1106.

A

```
Cx26   HEKKRKFIKGE---------IKSEFKDIEEI----------KTQKVRIEGSLWWTYTSSIFFRVIFEAAFMYVFYVM 157
Cx30   HETTRKFRRGE---------KRNDFKDIEDI----------KKQKVRIEGSLWWTYTSSIFFRIIFEAAFMYVFYFL 157
Cx32   HIE-KKMLRLE---------GHGDPLHLEEV----------KRHKVHISGTLWWTYVISVVFRLLFEAVFMYVFYLL 156
Cx43   RKE-EKLNKKEEELKVAQTDGVNVDMHLKQIEIKKFKYGIEEHGKVKMRGGLLRTYIISILFKSIFEVAFLLIQWYI 176
```

B

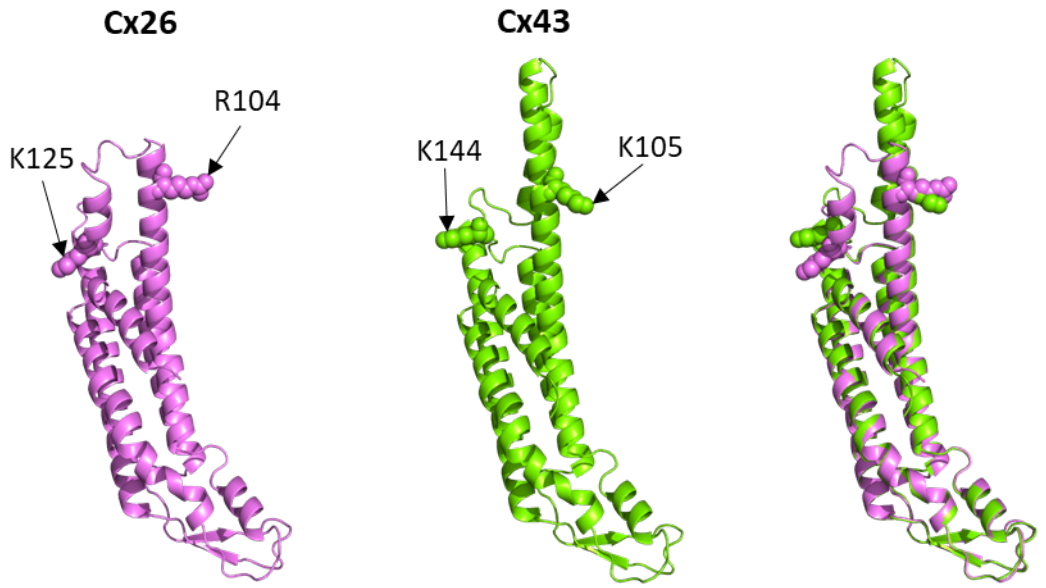

C

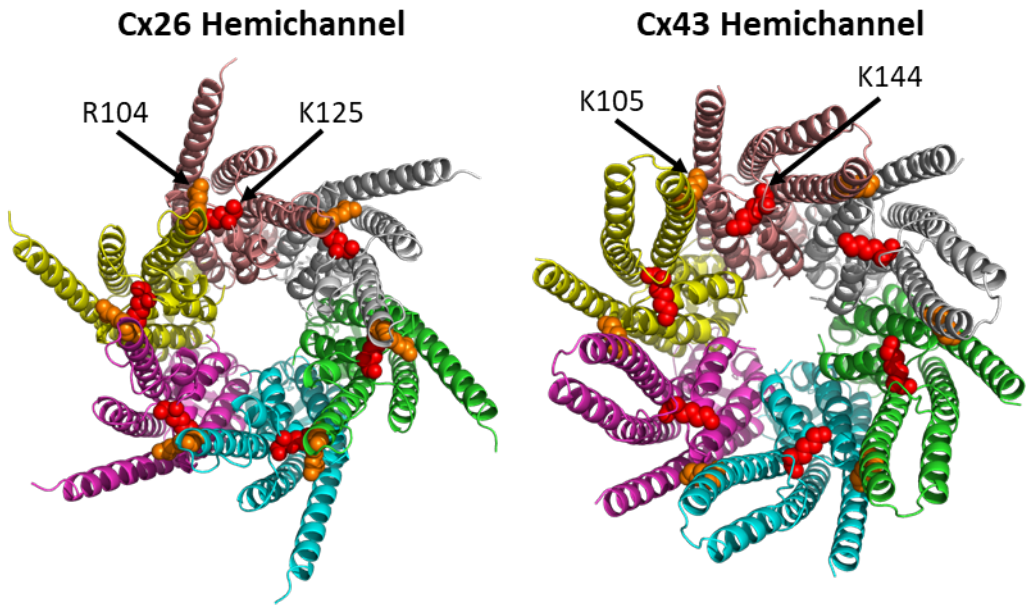

Figure 1: Structures of Cx43 and Cx26 predicted by AF3. (**A**) α- and β-connexin sequence alignment with the known CO_2-sensitive connexins at the top, Cx26, Cx30 and Cx32, followed by the α-connexin Cx43. The carbamylation motif is highlighted by the green box. (**B**) Cx26 and Cx43 AlphaFold3 structural alignments. (**C**) Cx26 and Cx43 hemichannel structural prediction.

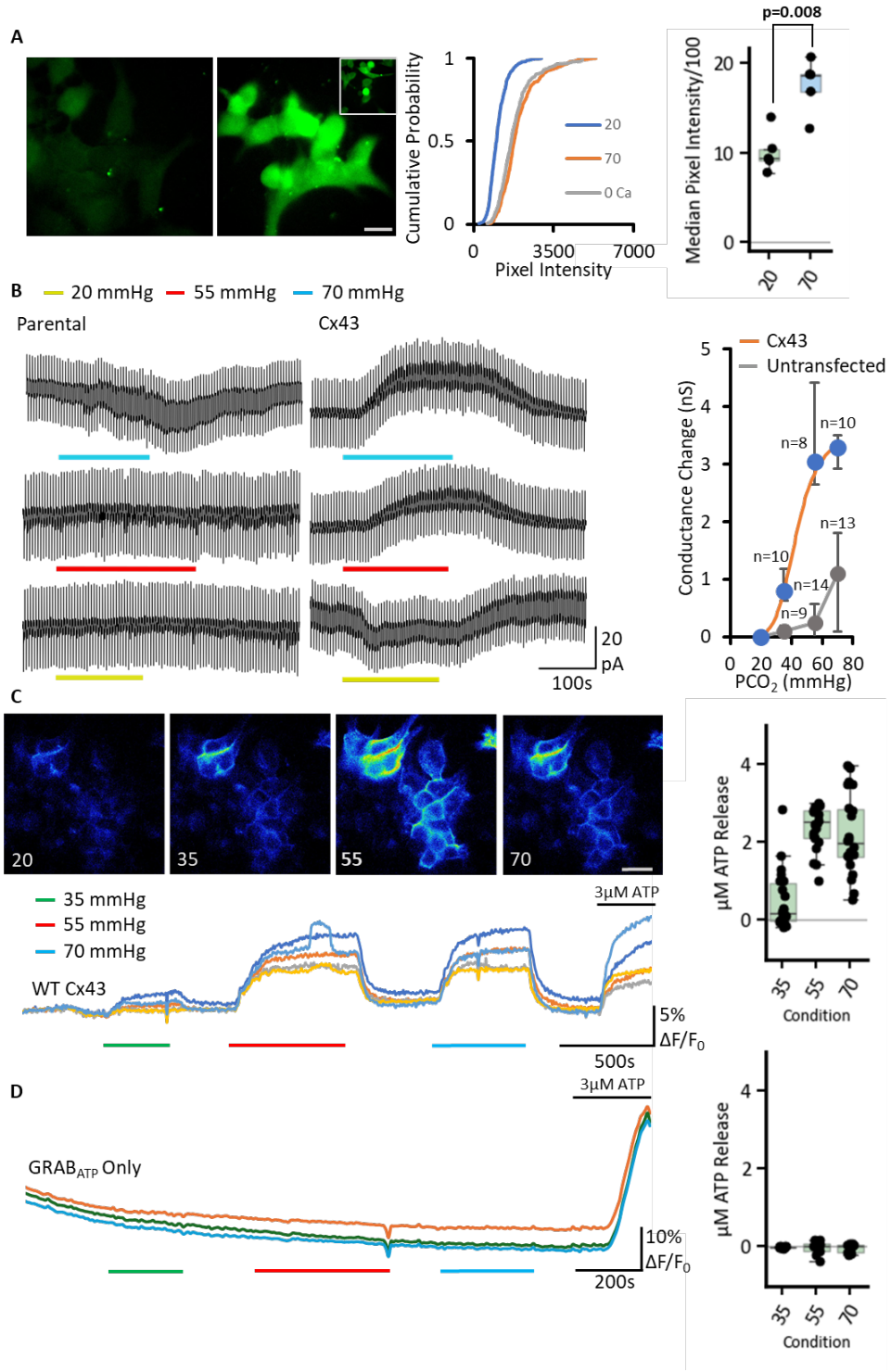

Figure 2: Cx43 hemichannels can be opened by an increase in PCO_2. The CO_2 sensitivity of Cx43 was assayed using three different methods. **(A)** Dye-loading with CBF from 20 (left) to 70 mmHg PCO_2 (right). The inset represents the 0 Ca^{2+} control, white scale bar is 20 μm. Cumulative probability graph represents all the data points measured with more than 200 cells per condition, box plot shows the medians from each independent transfection. **(B)** Electrophysiology voltage patch clamp was done on HeLa cells expressing Cx43. The baseline was set to 35 mmHg PCO_2 and three different concentrations were used (20, 55, 70 mmHg). The conductance change evoked by a change in PCO_2 was measured and plotted as a dose response curve

(right side, median with interquartile range) fitted by the Hill equation H=6, EC_{50}=43 mmHg. **(C)** The genetically-encoded ATP sensor $GRAB_{ATP}$ was co-transfected alongside Cx43 into HeLa cells (n=22). Representative images at different PCO_2 concentrations of the cells are shown, grey scale bar is 20 µm. Traces from the recording the images were selected from are shown; each line represent a different cell, the fluorescence was normalised by dividing all values by the baseline median pixel intensity before plotting. Box plot shows the µM ATP release as determined by normalisation to the 3 µM control solution applied. **(D)** HeLa cells transfected with $GRAB_{ATP}$ alone do not exhibit CO_2 dependent ATP release (n=14), summary box plot shows the µM ATP release as determined by normalisation to 3 µM ATP calibration.

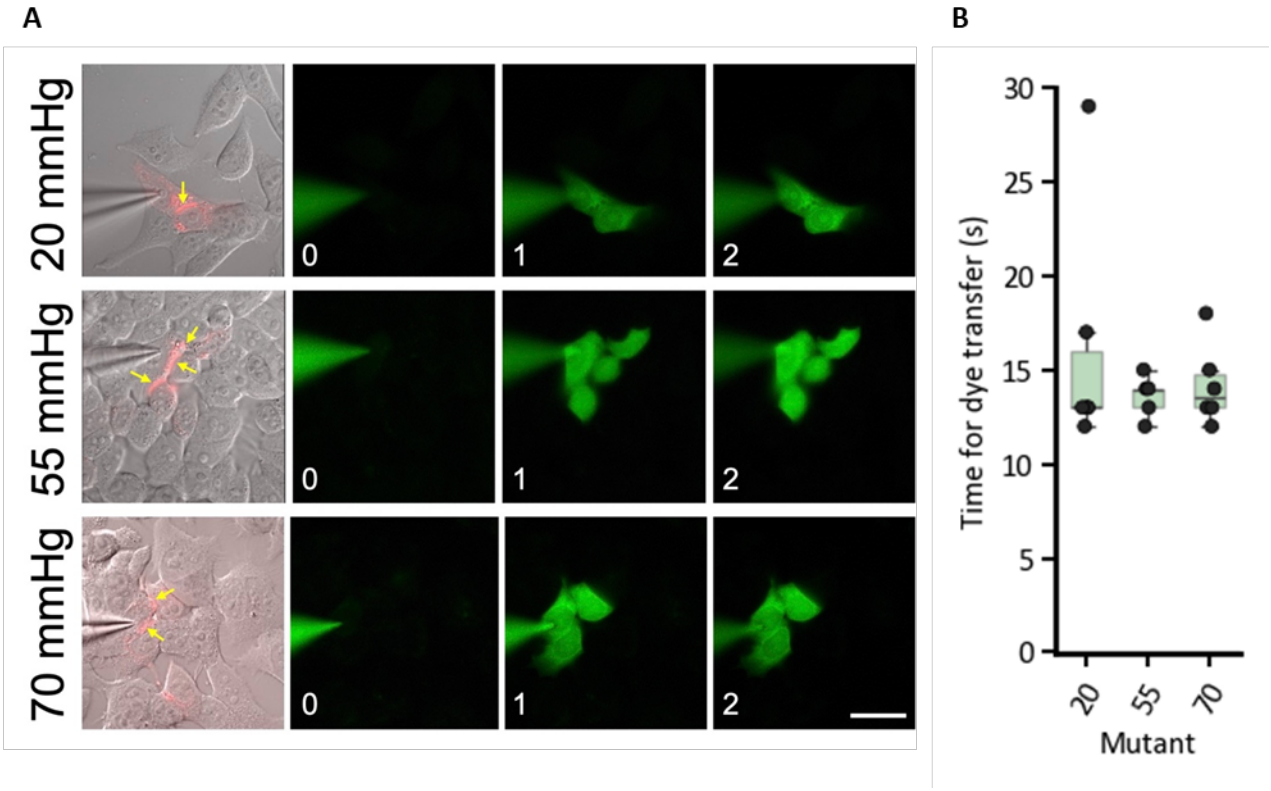

Figure 2, Figure supplement 1. Cx43 gap junction channels are insensitive to changes in PCO_2. A) DIC image with mCherry fluorescence superimposed. Gap junctions are evident as red stripes between cells (yellow arrows). The fluorescence images show the patch pipette filled with NBDG its loading into the recorded cell and the neighbouring cells coupled via gap junctions. The numbers in each bottom left corner are the time of the recording from whole cell breakthrough in minutes. Scale bar 20 µm. B) Summary graphs showing the time for the acceptor cell to reach 10% of the fluorescence of the donor cell at three different levels of PCO_2 (n=6 for each condition).

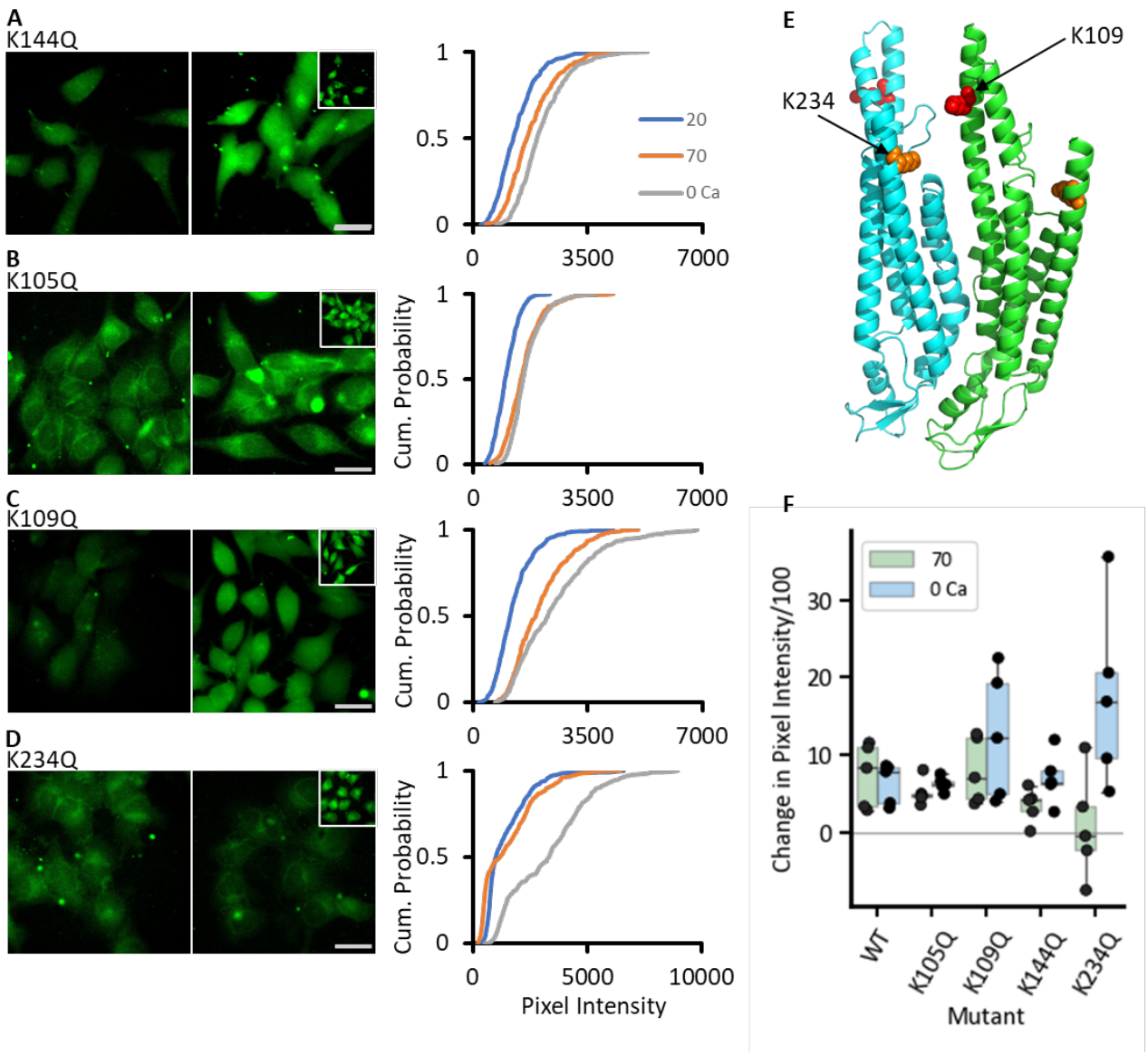

Figure 3: The effect of single Lys mutations on the CO_2 sensitivity of Cx43. HeLa cells transfected with the mutant variant of Cx43 were subjected to the dye-loading protocol. Images of dye loading in response to CO_2 and the 0 Ca^{2+} positive control, together with the cumulative probability plots are shown for K105Q (**A**), K109Q (**B**), K144Q (**C**), K234Q (**D**). **(E)** AlphaFold3 prediction of Cx43 with hypothesised carbamylation bridge residues highlighted – K234 in orange and K109 in red. **(F)** Summary box plots for dye-loading showing the change in median pixel intensity from 20 mmHg PCO_2 for each condition (70 mmHg PCO_2 – green and 0 Ca^{2+} blue, n=5) for WT (recalculated data from Fig 2A for comparison) and each mutation. Scale bars are 20 µm.

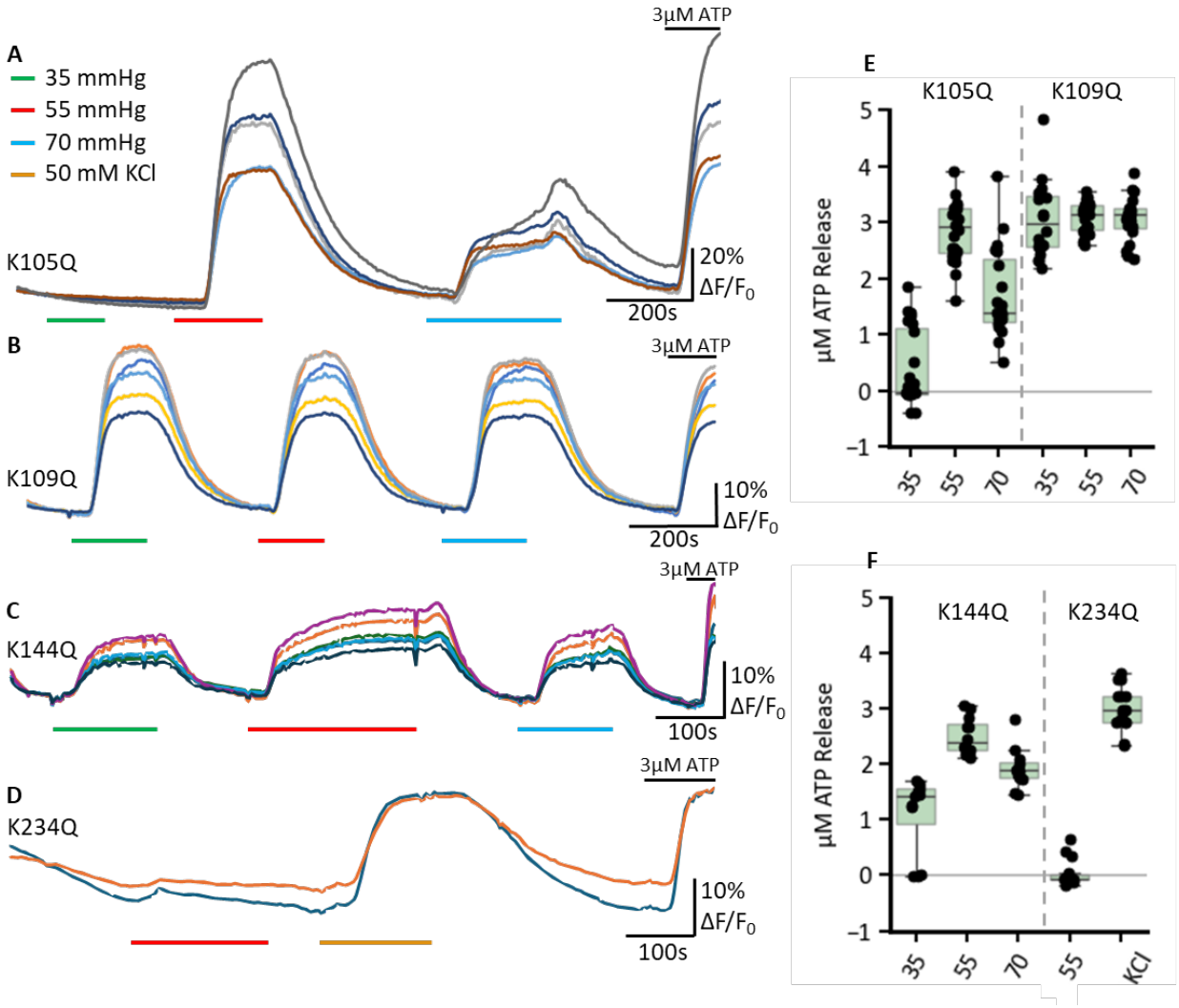

Figure 4: The effect of single Lys mutations on CO_2-dependent ATP release from Cx43. The genetically-encoded ATP sensor $GRAB_{ATP}$ was co-transfected alongside Cx43 mutant variations, K105Q (**A**) n=23, K109Q (**B**) n=20, K144Q (**C**) n=12, K234Q (**D**) n=15. Representative trace measurements were selected; each line represents a different cell; the fluorescence was normalised by dividing all values by the baseline median pixel intensity before plotting. Box plot on the right (**E**) and (**F**) represent the µM ATP released as determined through normalisation to the 3 µM ATP application.

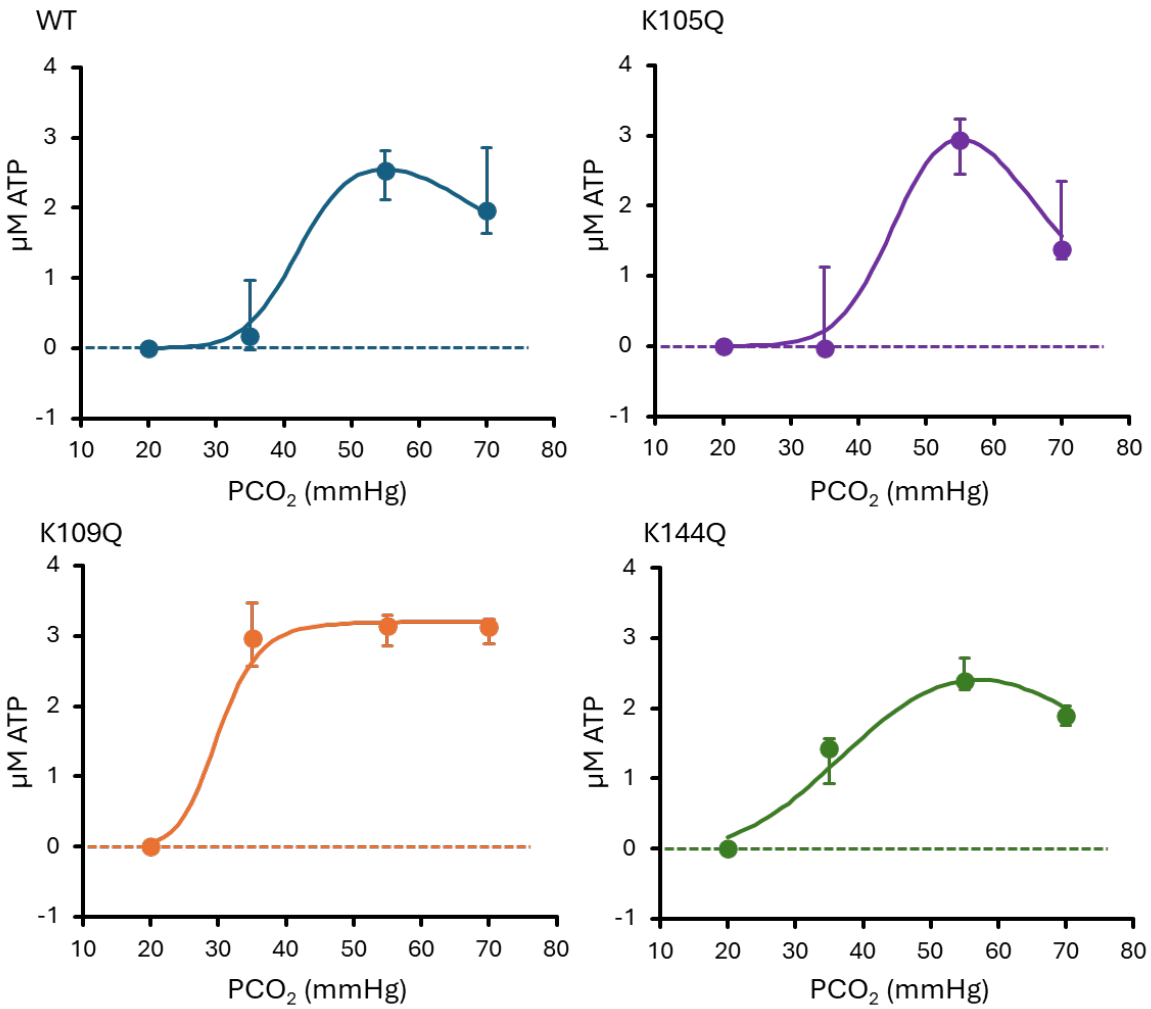

Figure 4, Figure supplement 1. The effect of single Lys mutations on the CO_2 dose-response properties of Cx43. Comparison of $Cx43^{WT}$ (data replotted from Fig 2C), $Cx43^{K105Q}$, $Cx43^{K109Q}$ (data replotted from Fig 4E) and $Cx43^{K144Q}$ (data replotted from Fig 4F). Data is plotted as medians with lower and upper quartiles. For the WT, K105Q and K144Q the fitted curve is drawn according to a modified Hill equation:

$$[ATP]=Max_{ATP}.\{([ATP]/K)^{H}/(1+([ATP]/K)^{H})\}.\{1-([ATP]/K_i)^{Hi}/(1+([ATP]/K_i)^{Hi})\}$$

Where K and H are the affinity and Hill coefficient of the channel for opening by CO_2, K_i and H_i are the affinity and Hill coefficient for inhibition of the channel by CO_2, and Max_{ATP} is the asymptotically maximum release of ATP to CO_2. For K109Q which did not exhibit CO_2-dependent inhibition at high levels of PCO_2, the Hill equation was used. The parameters for the curves are:

	$Cx43^{WT}$	**$Cx43^{K105Q}$**	**$Cx43^{K109Q}$**	**$Cx43^{K144Q}$**
Max_{ATP} (µM)	3.2	4.5	3.2	3.8
K (mmHg)	43	47	30	43
H	10	10	10	4
K_i (mmHg)	75	65	-	75
H_i	6	8	-	6

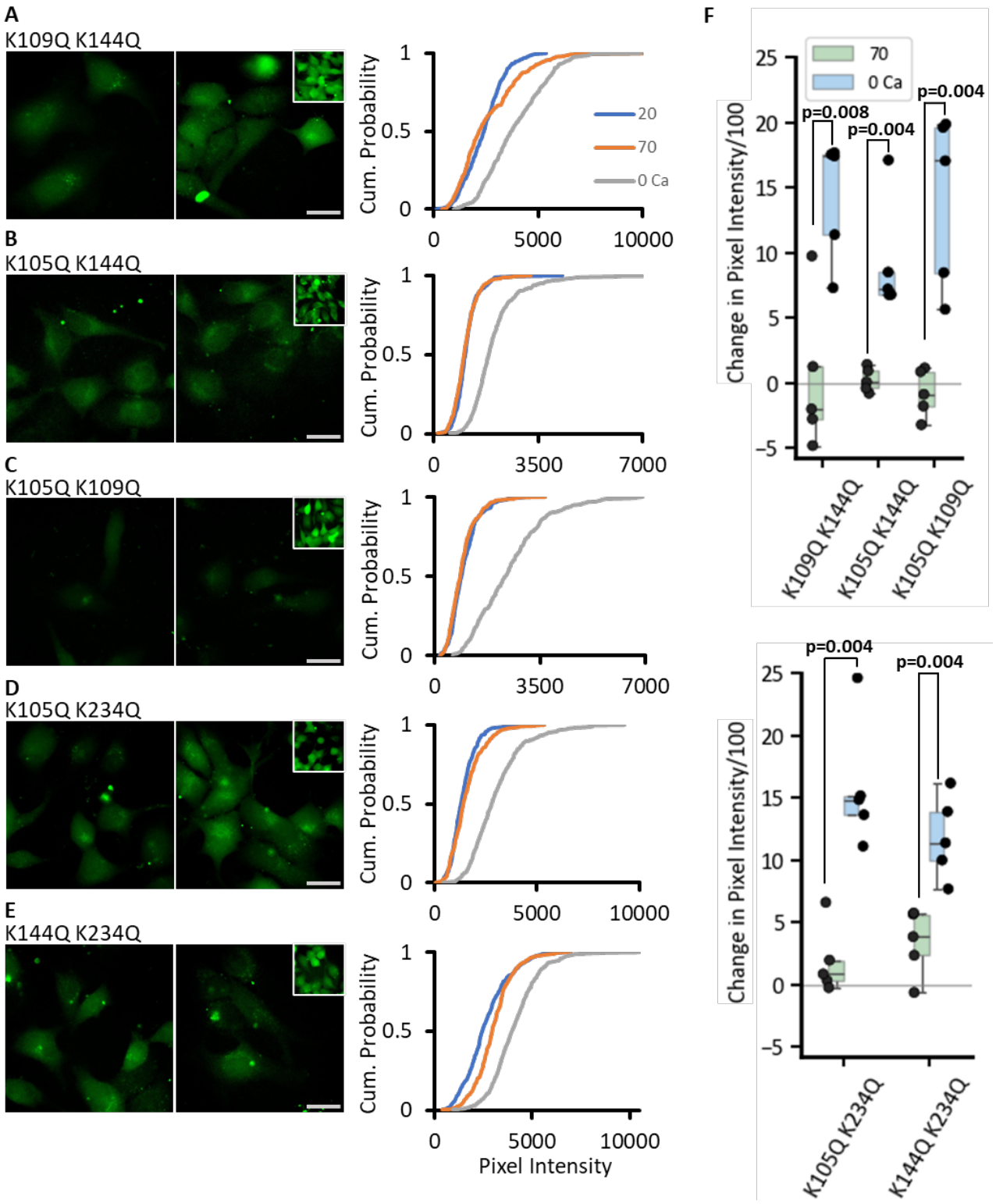

Figure 5: Paired Lys mutations are required to abolish the CO_2 sensitivity of Cx43. Expressing cells pixel intensity for each construct was measured from 5 individual transfections, with at least 40 cells per condition. Representative images for all combinations tried are shown – K109Q K144Q (**A**), K105Q K144Q (**B**), K105Q K109Q (**C**), K105Q K234Q (**D**), K144Q K234Q (**E**). Cumulative probability plots display all measured data points. The box plot shows the change in median pixel intensity from 20 mmHg PCO_2 for each transfection for 70 mmHg PCO_2 (green) and 0 Ca^{2+} (blue).

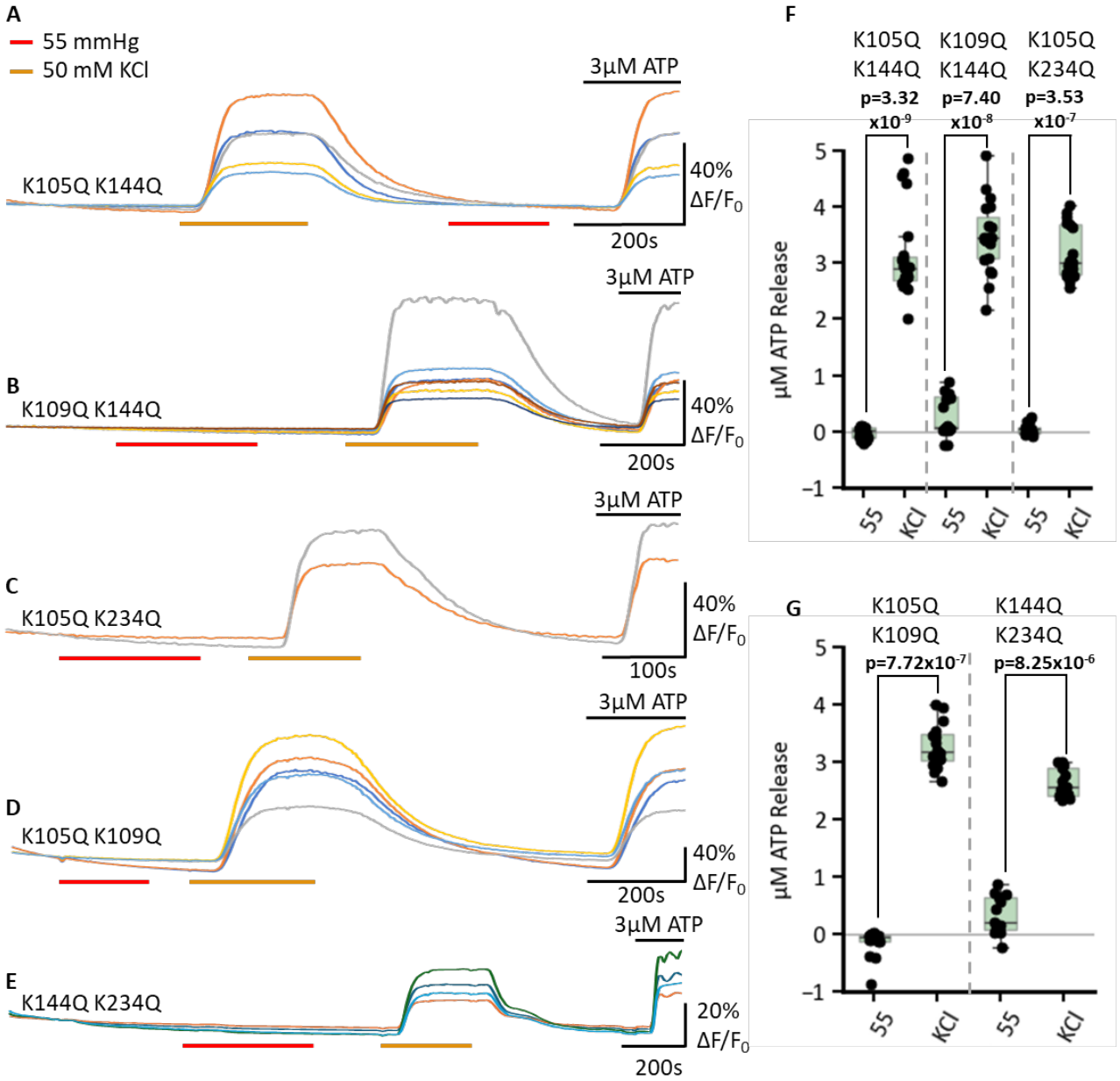

Figure 6: Paired Lys mutations abolish CO_2 dependent ATP release via Cx43. HeLa cells co-expressing Cx43 and $GRAB_{ATP}$ were subjected to changing PCO_2-levels and fluorescence was recorded . Representative traces (**A-E**) for each of the Cx43 mutations – K105Q K144Q (**A**) n=23, K109Q K144Q (**B**) n=19, K105Q K234Q (**C**) n=17, K109Q K234Q (**D**) n=16, K144Q K234Q (**E**) n=13. The traces indicate normalised fluorescence changes ($\Delta F/F_0$). 3 µM ATP was applied at the end of each experiment to confirm sensor functionality. Furthermore, as a positive control, 50 mM KCl was applied to depolarise the cells and confirm channel function. (**F-G**) Box plots summarising the total ATP release in µM for each double mutant in 55 mmHg PCO_2 and 50 mM KCl. Data points represent individual measured cells.

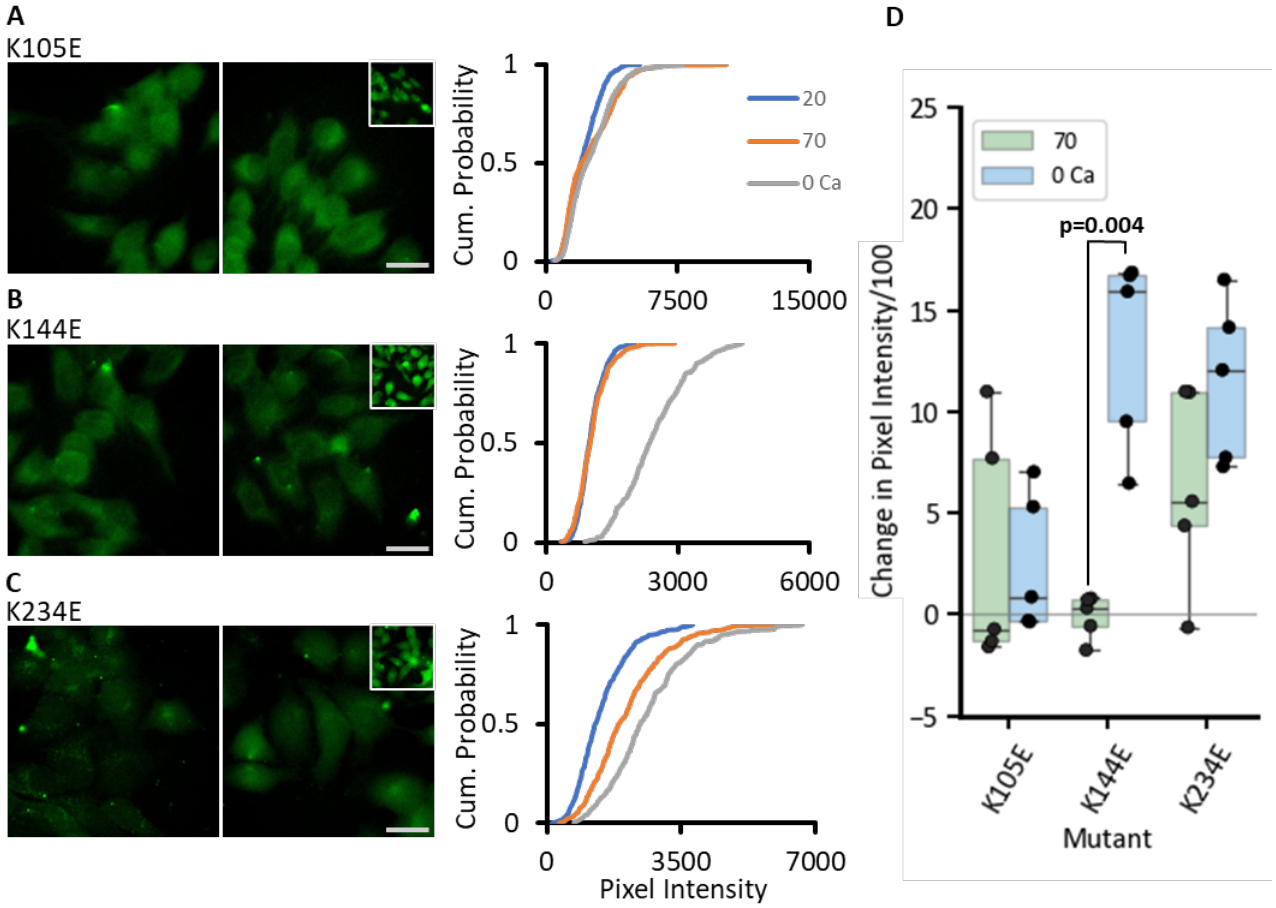

Figure 7: Introduction of negative charge into the carbamylation motif via Lys to Glu mutations has mixed effects on CO_2 sensitivity of Cx43 hemichannels. Expressing cells pixel intensity for each construct was measured from 5 individual transfections, with at least 40 cells per condition. (**A-C**) Representative cell images for 20 (left), 70 (right) with insets displaying the 0 Ca^{2+} control for each mutant K105E (**A**), K144E (**B**), K234E (**C**). Scale bar represents 20 µm. Cumulative probability graphs of pixel intensities are shown on the right for each mutant with three conditions 20 mmHg PCO_2 (blue line), 70 mmHg PCO_2 (orange) and 0 Ca^{2+} (grey line). The box plot shows change in median pixel intensity from 20 mmHg PCO_2 for each transfection for 70 mmHg PCO_2 (green boxes) and 0 Ca^{2+} (blue boxes).

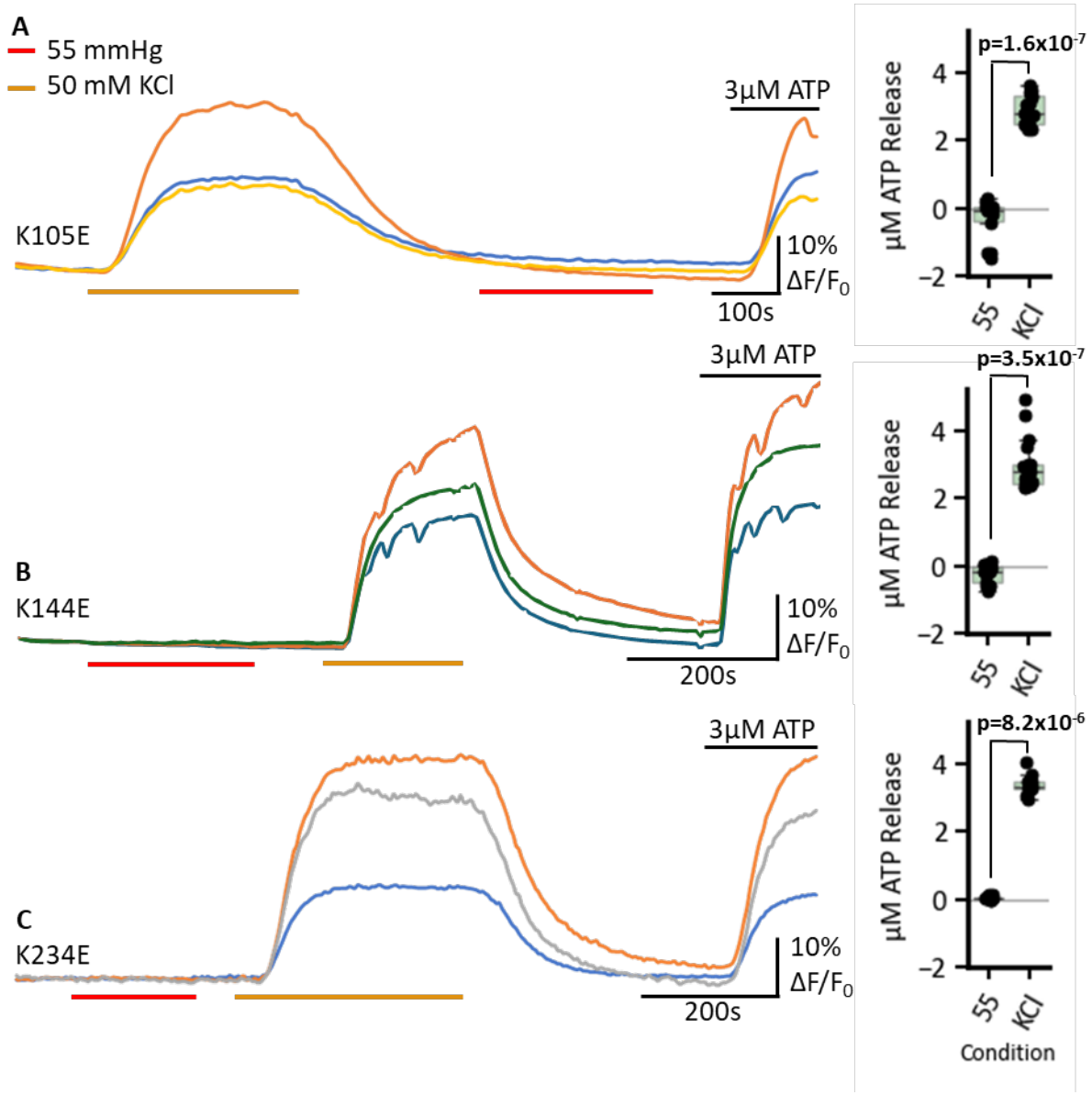

Figure 8: Lys to Glu mutations abolish CO_2-dependent ATP Release. $GRAB_{ATP}$ fluorescence traces of ATP release from cells expressing single mutant connexins: K105E (**A**) n=18, K144E (**B**) n=17, K234E (**C**) n=13, in response to 55 mmHg PCO_2 (red bars), 50 mM KCl depolarisation control (orange bars) and a 3 µM ATP control application at the end of all experiments to confirm sensor functionality. Traces show changes in normalised fluorescence over time (ΔF/F), indicating ATP release. On the right, the box plots display the quantified ATP release in µM for each mutant under 55 mmHg PCO_2 and 50 mM KCl. Each data point represents a measurement from an individual cell.

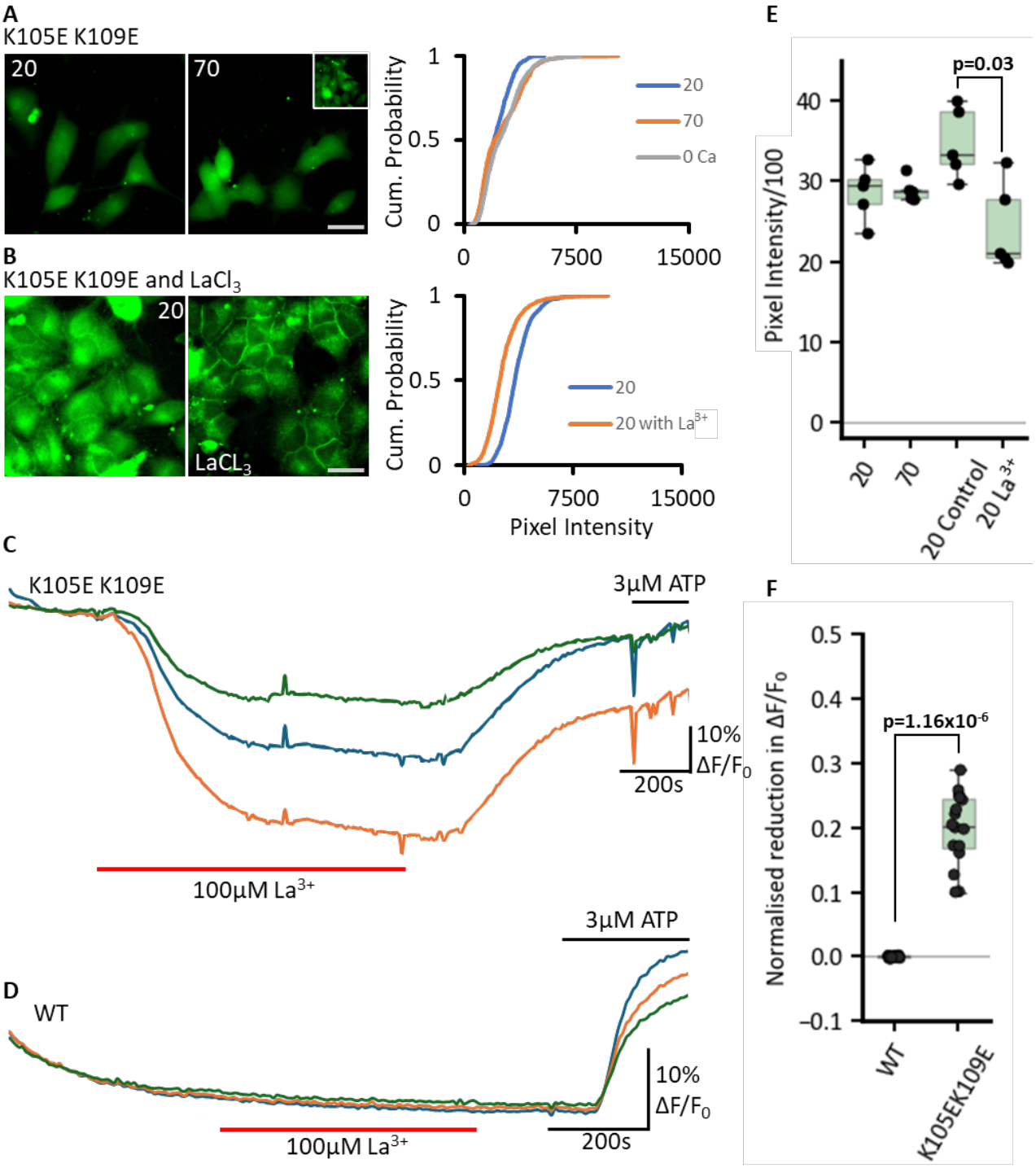

Figure 9: The Cx43 double mutant, K105E K109E, is constitutively open. (**A**) Representative fluorescence images of cells expressing the Cx43 K105E K109E mutant under low (20 mmHg PCO_2, left) and high CO_2 (70 mmHg PCO_2, right), an inset showing the 0 Ca^{2+} control is present. Scale bar = 20 µm. Cumulative probability plot of pixel intensity for each condition is shown on the right, overall indicating higher baseline fluorescence and perpetually open hemichannels. (**B**) Dye-loading with 20 mmHg PCO_2 (left) and 20mmHg PCO_2 with 100 µm $LaCl_3$. Cumulative probability plot for pixel intensity under these conditions is shown on the right. (**C**) Fluorescence traces of ATP release from cells co-expressing $GRAB_{ATP}$ and Cx43 K105E K109E (n=16) under 20 mmHg PCO_2 and 20 mmHg PCO_2 with 100 µM $LaCl_3$ (red bar). Fluorescence

is normalised to baseline. (**D**) Fluorescence traces of ATP release from cells co-expressing $GRAB_{ATP}$ and Cx43 WT under 20 mmHg PCO_2 and 20 mmHg PCO_2 with 100 µM $LaCl_3$ (red bar). (**E**) Box plots summarizing median pixel intensity under the different conditions, showing a significant reduction in intensity in the presence of $LaCl_3$ ($p = 0.03$). (**F**) Box plot shows normalised fluorescence changes values for the difference between – 20 mmHg PCO_2 (representing baseline normalisation) and the application of $LaCl_3$ for both the K105E K109E and WT Cx43 constructs.

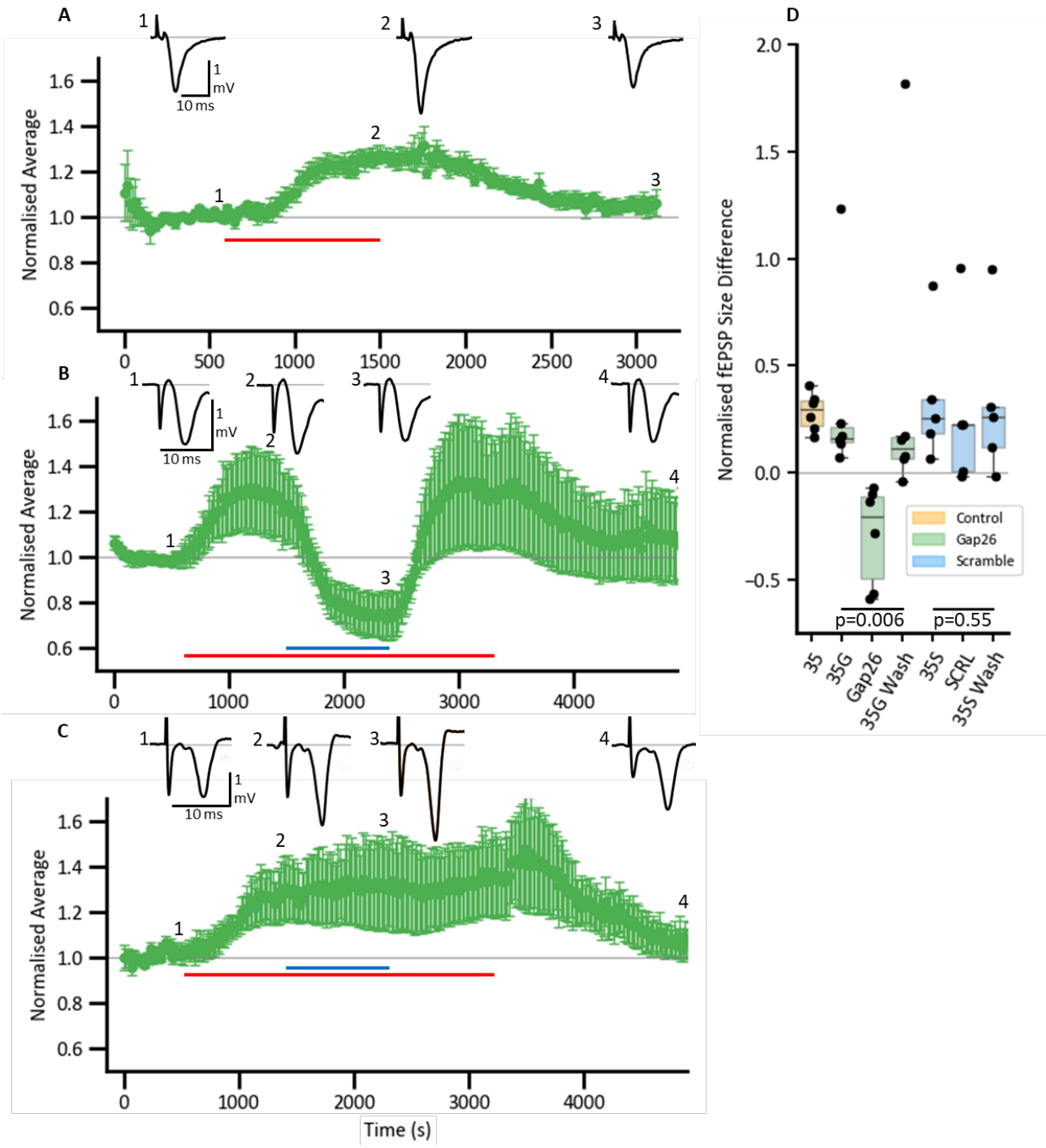

Figure 10: PCO_2-dependent modulation of amplitude of fEPSPs in hippocampus is mediated via Cx43. (**A-C**) Time-course plots showing the average amplitude of the normalised fEPSP (± SEM) amplitude in response to different conditions. Inserts display representative fEPSPs. (**A**) Control condition showing an increase in fEPSP amplitude in response to a modest change to PCO_2 (20 to 35 mmHg), red bar represent the application of 35 mmHg PCO_2, baseline conditions – 20 mmHg PCO_2. (**B**) EPSP responses in the presence of Gap26 (blue bar) and subsequent wash. (**C**) EPSP responses with scrambled Gap26 peptide applied (blue bar). (**D**) Box plots representing the normalised fEPSP size difference (baseline was subtracted) with colour coded conditions: orange – control 35 mmHg PCO_2, green – Gap26 with pre (35G), after (35S Wash).

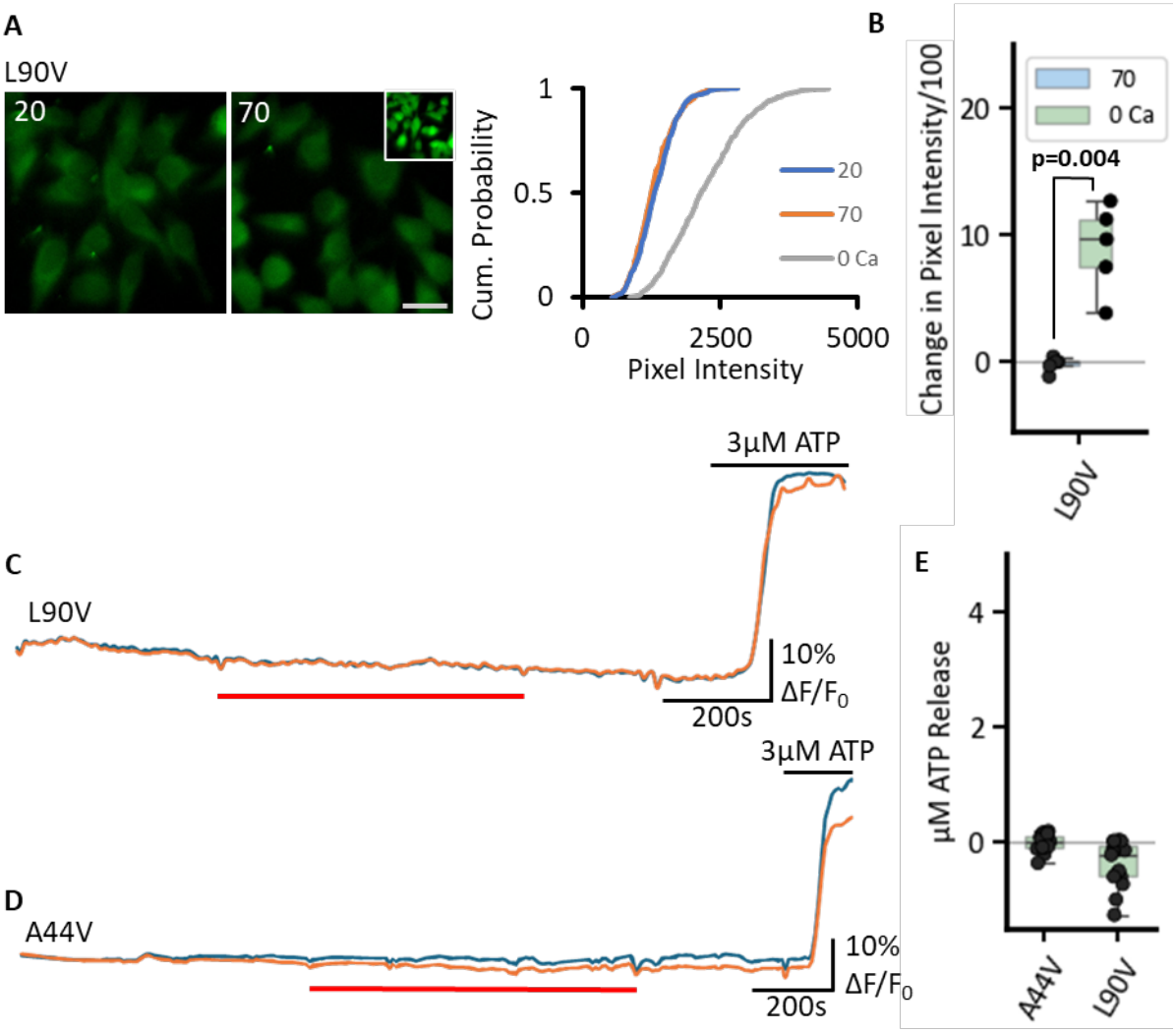

Figure 11. Pathological mutations of Cx43 remove its sensitivity to CO_2. A,B) L90V prevents CO_2-dependent dye loading. The dye loading assay shows no change in fluorescence between 20 and 70 mmHg, yet functional channels are expressed as shown by the zero Ca^{2+} positive control. Box plot shows the change in median pixel intensity from 20 mmHg PCO_2 for each transfection for 70 mmHg PCO_2 (green boxes) and 0 Ca^{2+} (blue boxes). **C-E)** $GRAB_{ATP}$ recordings shown that L90V and A44V also abolish CO_2-dependent ATP release.